March 20, 2014
TPF-5(264) Passive Force/Skewed Abutments
Task 8 Preliminary Report

TASK 8 REPORT

PASSIVE FORCE-DEFLECTION TESTS FOR 3 FOOT UNCONFINED SKEWED ABUTMENTS

Prepared By

Kyle M. Rollins, Professor, Civil & Env. Engrg Dept., Brigham Young Univ., 368 CB, Provo, UT 84602, (801) 422-6334, rollinsk@byu.edu

Ian Oxborrow, Research Asst., Civil & Env. Engrg Dept., Brigham Young Univ., 368 CB, Provo, UT 84602; i.oxborrow@gmail.com

Kyle Smith, Research Asst., Civil & Env. Engrg Dept., Brigham Young Univ., 368 CB, Provo, UT 84602, kyle.smith@byu.net

Amy Fredrickson, Research Asst., Civil & Env. Engrg Dept., Brigham Young Univ., 368 CB, Provo, UT 84602, af711.byu@gmail.com

Arthur Guo, Research Asst., Civil & Env. Engrg Dept., Brigham Young Univ., 368 CB, Provo, UT 84602, gzifan@gmail.com

Katie Palmer, Research Asst., Civil & Env. Engrg Dept., Brigham Young Univ., 368 CB, Provo, UT 84602, katienpalmer@gmail.com

Prepared for

Research Division of the Utah Department of Transportation

March 20, 2014

EXECUTIVE SUMMARY

Accounting for seismic forces and thermal expansion in bridge design requires an accurate passive force-deflection relationship for the abutment wall. Current design codes make no allowance for skew effects on passive force; however, quarter scale lab tests indicate that there is a significant reduction in peak passive force as skew angle increases for plane-strain cases. Large scale tests also indicate the same phenomena for plane-stress cases. All previous tests had been performed with backwall width to height (W/H) ratios of 2.0. To more completely explore this issue, tests were performed with larger width to height ratios. The abutment backwall was still 11-ft (3.35-m) wide by 5.5-ft (1.68-m) high, but the backfill was only 3 high against the backwall creating a W/H ratio of 3.7. The backfill material consisted of dense compacted sand. The peak passive force for the 15°, 30°, and 45° skew tests was found to be 71%, 44%, and 35%, respectively of the peak passive force for the 0° skew case. These results are in very good agreement with previous laboratory and field tests, suggesting that the W/H ratios have relatively little effect on the reduction factor. Passive forces peaked at deflections between 3% and 4% of the backwall height which is consistent with past testing on non-skewed abutments. Passive pressure across the backwall was initially uniform but became non-uniform at larger displacements with higher pressures near the edges of the wall and the highest values at the obtuse corner. Shear force on the backwall increased as skew angle increased despite the reduction in longitudinal force with skew angle. Transverse pile cap displacement also increased with skew angle and was sufficient to mobilize the frictional resistance. Heave geometries for the 0°, 15°, 30°, and 45° tests were 5% to 11% of the fill height. In plan view, the shear surface extended nearly parallel to the backwall face on the acute side of the wall and normal to the backwall face on the obtuse side. In all cases, the failure surface extended beyond the edge of cap increasing the effective with of the abutment to approximately 17 to 19 ft (5.2 to 5.8 m). The failure surface typically daylighted at about 9 ft (2.75 m) in front of the face of the cap when measured perpendicular to the backwall.

INTRODUCTION

Numerous large-scale experiments have been conducted with the intent to determine the passive force-deflection curves that might be expected for dense compacted fill behind non-skewed bridge abutments (Mokwa and Duncan 2001; Rollins and Cole 2006; Rollins et al. 2010; Rollins and Sparks 2002). Much of this research indicates that the peak passive force can be accurately predicted using the log-spiral method and is achieved at a longitudinal deflection of 3% to 5% of the backwall height (Rollins and Cole 2006). Methods approximating the complete passive force-deflection curve with a hyperbola have been developed by Shamsabadi et al. (2007) and Duncan and Mokwa (2001). However, for simplicity in design, most specifications recommend a bilinear relationship (AASHTO 2011; Caltrans 2001).

Until recently, no large-scale experiments had been conducted to determine the passive force-deflection relationships for skewed bridge abutments. Furthermore, current bridge design practices assume the peak passive force is the same for skewed bridges as for non-skewed bridges (AASHTO 2011). However, field evidence clearly indicates poorer performance of skewed abutments during seismic events (Apirakyorapinit et al. 2012; Elnashai et al. 2010; Shamsabadi et al. 2006; Unjohn 2012) and distress to skewed abutments due to thermal expansion (Steinberg and Sargand 2010). Laboratory tests performed by Rollins and Jessee (2012) and numerical analyses performed reported by Shamsabadi et al. (2006) both found that there is a significant reduction in passive force as skew angle increases. Using data obtained from these studies, Rollins and Jessee (2012) proposed the correction factor, R_{skew}, given by Equation (1) which defines the ratio between the peak passive force for a skewed abutment ($P_{P\text{-}skew}$) and the peak passive force for a non-skewed abutment ($P_{P\text{-}no\ skew}$) as a function of skew angle, θ.

$$R_{skew} = P_{P-skew} / P_{P-no\ skew} = 8.0 * 10^{-5}\theta^2 - 0.018\theta + 1.0 \quad (1)$$

To more fully understand the relationship between skew angle and reduction in peak passive force, four large-scale tests were conducted to determine the passive force-deflection curves for skew angles of 0°, 15°, 30°, and 45°. Tests with 0°, 15°, and 30° skew angles were performed in 2012. The 45°

skew test was part of this study. All four tests were conducted using an existing 11-ft (3.35-m) wide by 5.5-ft (1.68-m) high by 15-ft (4.57-m) long pile cap which has been used for a number of previously conducted lateral load and passive force-deflection tests (Rollins et al. 2010; Rollins and Sparks 2002; Strassburg 2010). The 0° skew test for this study was conducted in a similar fashion to the tests conducted by the previous researchers. For the 15°, 30°, and 45° skew tests a concrete wedge was attached to the face of the existing pile cap. Testing procedures, results, comparisons to available results and recommendations based on analysis of the test results are presented in this paper.

BACKGROUND

As outlined by Burke Jr. (1994) and shown in Figure 1, the interaction of forces at the interface between the bridge abutment backwall and soil backfill may be expressed in terms of the total longitudinal force, P_L, and its components normal to and transverse to the abutment. The normal force is resisted by the passive force, P_P [see Equation (2)]; and the transverse, or shear force, P_T [see Equation (3)], is resisted by the shear resistance, P_R [see Equation (4)]. To prevent instability of the bridge caused by sliding of the abutment against the soil backfill the inequality shown in Equation (5) must be satisfied. In addition, rotation of the entire bridge can occur if the inequality in Equation (6) is not satisfied.

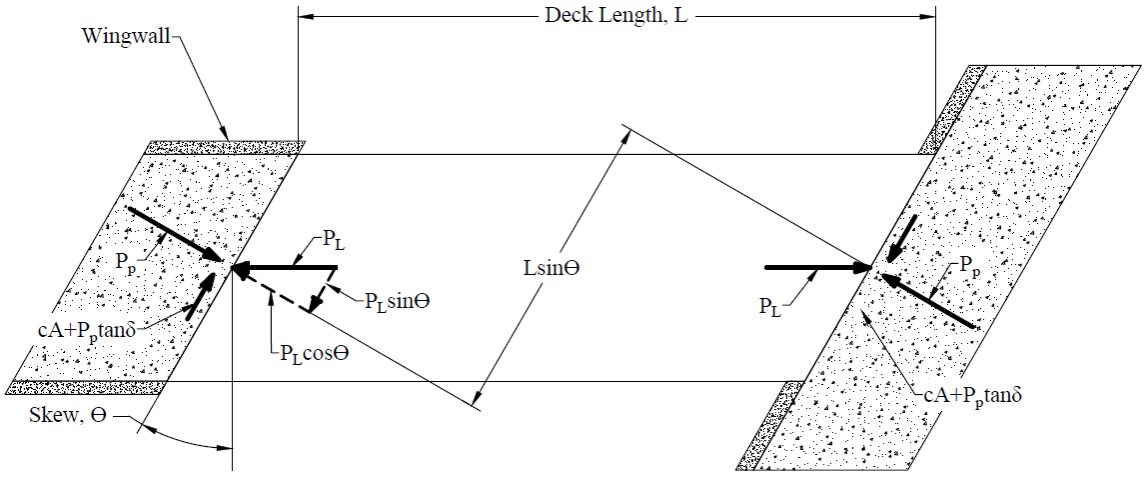

Figure 1. Typical distribution of forces on a bridge with skewed abutments.

$$P_P = P_L \cos\theta \quad (2)$$

$$P_T = P_L \sin\theta \quad (3)$$

$$P_R = cA + P_P \tan\delta \quad (4)$$

$$\frac{cA + P_P \tan\delta}{F_s} \geq P_L \sin\theta \quad (5)$$

$$\frac{(cA + P_P \tan\delta) L \cos\theta}{F_s} \geq P_P L \sin\theta \quad (6)$$

where

θ = skew angle of backwall

c = soil cohesion

A = backwall area

δ = angle of friction between backfill soil and abutment wall

F_s = factor of safety

L = length of bridge

These equations are only strictly valid if the bridge remains stable; therefore, if the bridge rotates, the distribution of forces on the abutment backwall will likely change, rendering these equations less accurate. Based on Equation (6), Burke Jr. (1994) noted that if cohesion is ignored the potential for bridge rotation is independent of passive force and bridge length so that at a typical design interface friction angle of 22°, the factor of safety decreases to below 1.5 if bridge skew exceeds 15°.

TEST CONFIGURATION

Test Geometry

The test setup for the lab tests is shown in Figure 2 and involved a 2 ft (0.61 m) high by 4 ft (1.22 m) wide backwall with a 2D or plane-strain backfill geometry (Rollins and Jessee 2012). In contrast, the field tests used an existing 11 ft (3.35 m) wide by 5.5 ft (1.68 m) high by 15 ft (4.57 m) long pile cap to simulate an abutment backwall as shown in Figure 3. Instead of a 2D backfill geometry, the backfill was placed in a test pit that extended a little over 5 ft (1.52 m) out from the sides of the pile cap to the edge of

the test pit with transverse concrete wingwalls to allow for the development of a 3D failure geometry. The backfill extended 24 ft (7.32 m) longitudinally from the face of the pile cap and approximately 1 ft (0.30 m) below the bottom of the cap from the face to 10 ft (3.05 m) from the face to contain the potential failure surface. Though the native soil was significantly stiffer than the backfill materials, the backfill boundaries were considered to be far enough away to not affect the development of a shear surface. Beyond 10 ft (3.05 m), the base of the backfill tapered up to be approximately even with the base of the cap to reduce the required backfill volume.

Load was applied in the longitudinal direction with two 600-kip (2,670 kN) hydraulic actuators which reacted against a sheet pile wall and two 4-ft (1.22 m) diameter drilled shafts that were coupled together by two deep beams.

Concrete wedges were attached to the front face of the pile cap to achieve skew angles of 15°, 30°, and 45°. Rollers were placed beneath the wedge to eliminate base friction resistance.

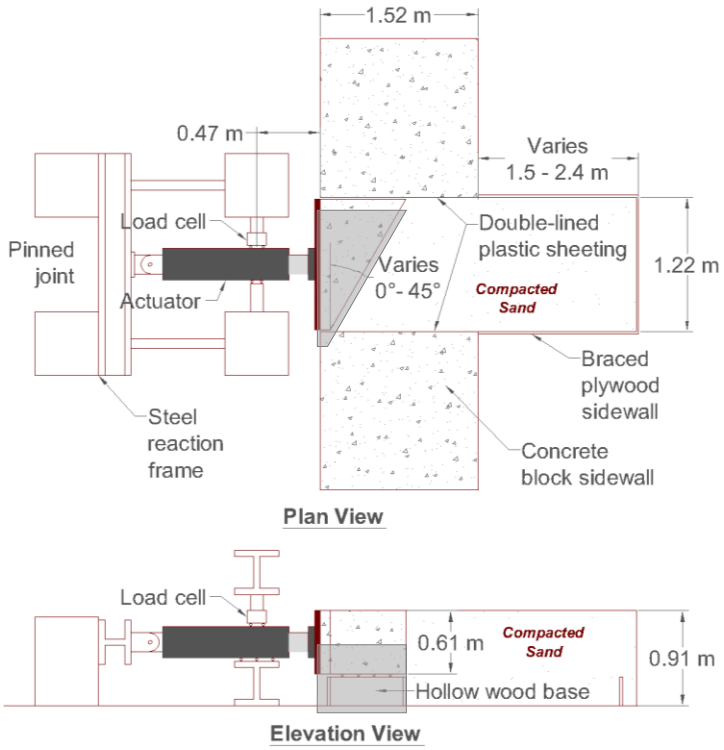

Figure 2. Schematic drawings of lab test layout (Rollins and Jessee 2012) (NOTE 1 m = 3.281 ft).

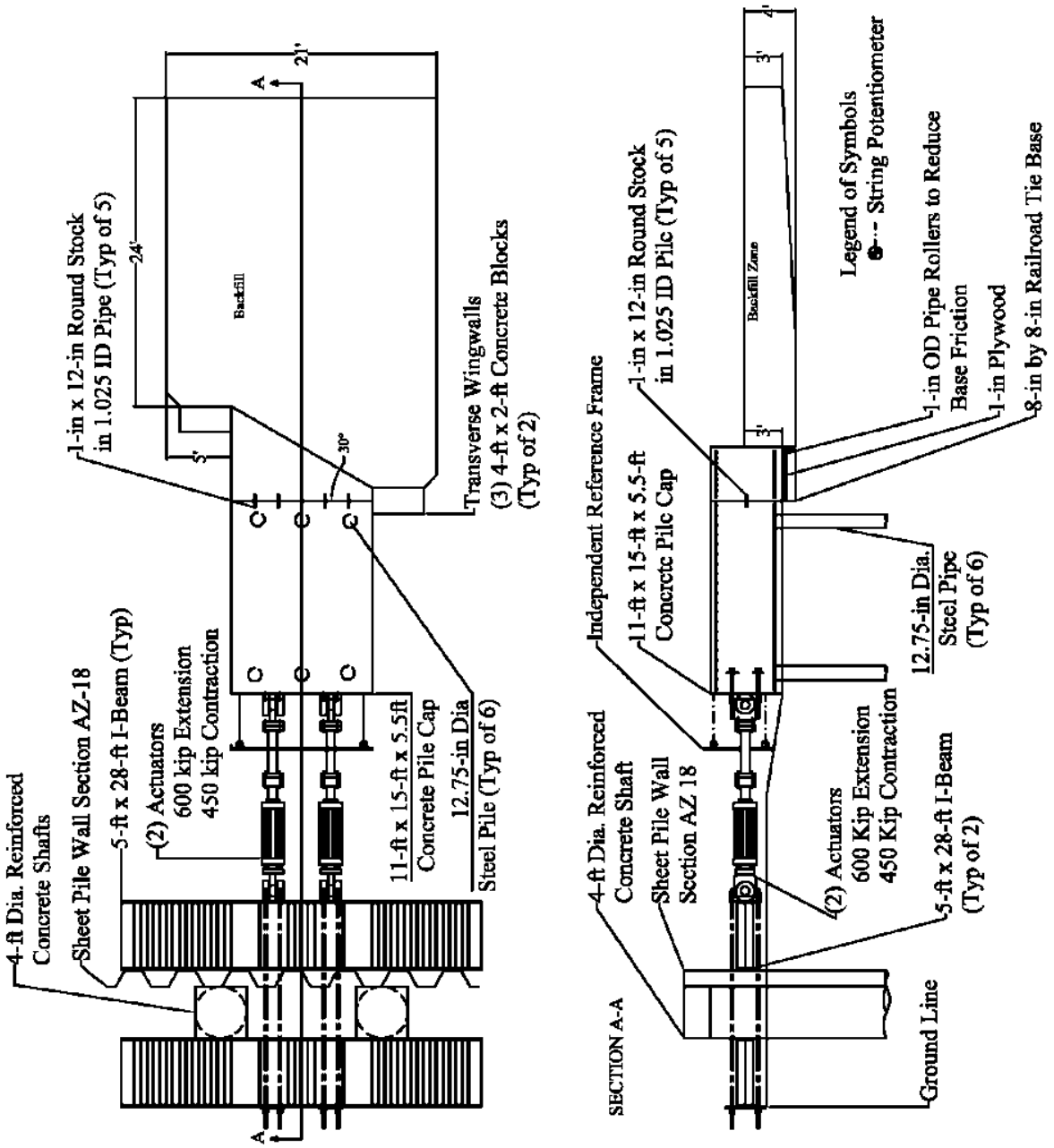

Figure 3. Schematic drawing of field test setup.

Instrumentation

Longitudinal load was measured using pressure transducers in the actuators. Longitudinal displacement of the pile cap was measured using four string potentiometers (string pots) located at each corner of the back of the pile cap and were tied to an independent reference frame. As the piles were assumed to provide vertical restraint, vertical movement of the pile cap was not monitored. Longitudinal

and transverse deflection versus displacements data profiles were measured using inclinometers and shape accelerometer arrays which extended approximately 40 ft (14 m) into the center pile in the North and South sides of the pile cap. The shape arrays provided data at 1 ft (0.30 m) intervals while the inclinometers provided data at 2 ft (0.6 m) intervals. Because of the time required to obtain inclinometer readings, the inclinometer measurements were only taken immediately before the start of a test and after the last deflection increment. In contrast, the shape arrays provided profiles at each deflection increment because their collection was instantaneous.

To measure backfill heave a 2 ft (0.61 m) grid was painted on the backfill surface and the relative elevation of each grid intersection was measured with a survey level and a total station prior to, and after conducting each test. Surface cracks in the backfill were also marked following the completion of each test. A hand auger was used to drill 2-in (51-mm) diameter, vertical holes at various locations through the backfill in order to determine the location of the internal failure surfaces. These holes were then refilled and compacted with red-dyed sand.

Following final pile cap displacement, a trench was excavated adjacent to these holes and the offset in the sand columns identified the locations of the failure surfaces.

Geotechnical Backfill Properties

Backfill materials consisted of a poorly-graded sand (SP or A-1-b as classified by the Unified Soil Classification System or AASHTO classification system, respectively). The particle-size distribution generally falls within the gradation limits for washed concrete sand (ASTM C33) as shown in Figure 4. Gradations before and after the test series found that the coefficient of uniformity (C_u) and coefficient of curvature (C_c) were 7.6 and 0.8 pre-test, and 9.7 and 0.7 post-test, respectively. This variability is likely due to small differences in soil samples. For comparison, the C_u and C_c values from the lab tests were 3.7 and 0.7, respectively. Figure 4 also shows the soil gradation for the lab tests.

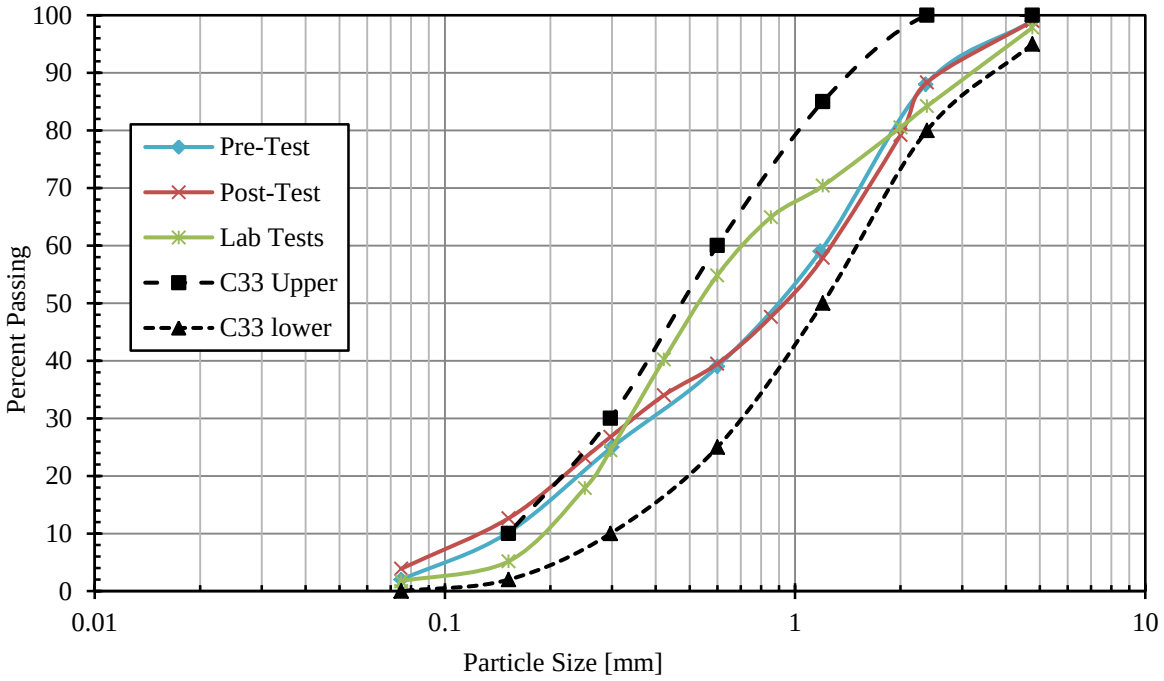

Figure 4. Gradation for backfill sand relative to concrete sand gradation.

Unit Weight and Moisture Content

Maximum dry unit weight according to the modified Proctor compaction test (ASTM D1557) performed prior to testing was 111.5 lbf/ft^3 (17.52 kN/m^3) and the optimum moisture content was 7.1%. The target on-site compaction level was 95% of the modified Proctor maximum. Backfill sand was placed in lifts approximately 6-in (15.24-cm) thick and compacted with a smooth-drum vibratory roller and a walk-behind vibratory plate compactor to an average density greater than approximately 95% of the modified Proctor maximum. A nuclear density gauge was used to obtain relative compaction and water content data during compaction. Though not shown, the variation of relative compaction and moisture content with depth was not significant. Relative density was estimated using the empirical relationship between relative density (D_r) and relative compaction (R) for granular materials developed by Lee and Singh (1971) as shown in Equation (7) where D_r and R are measured in percent.

$$R = 80 + 0.2D_r \quad (7)$$

A summary of the soil density and water content measurements for the four tests is shown in Table 1. The properties of the two backfills were generally very consistent. Average relative compaction, relative density, and water content for the three tests were 96.8%, 84%, 8.9%, respectively. For comparison purposes the average relative compaction, relative density, and water content for the laboratory tests were 97.9%, 90%, and 8.0%, respectively (Rollins and Jessee 2012).

TABLE 1 Summary of Compaction and Water Content Data for Each Test	*0° Test* *[pcf]*	*15° Test* *[pcf]*	*30° Test* *[pcf]*	*45° Test* *[pcf]*	*Average*
Minimum Measured Dry Unit Weight	105.7	105.9	105.7	105.9	105.8
Maximum Measured Dry Unit Weight	110.1	110.1	109.7	112.1	110.5
Average Dry Unit Weight	107.03	108.06	107.5	109.2	107.9
Average Moisture Percentage	9.3	9.5	9.6	7.1	8.9
Average Proctor Percentage	96.0%	96.9%	96.4%	97.9%	96.8%

Figure 5 through Figure 8 show the distribution of dry unit weight measurements during compaction for all four tests.

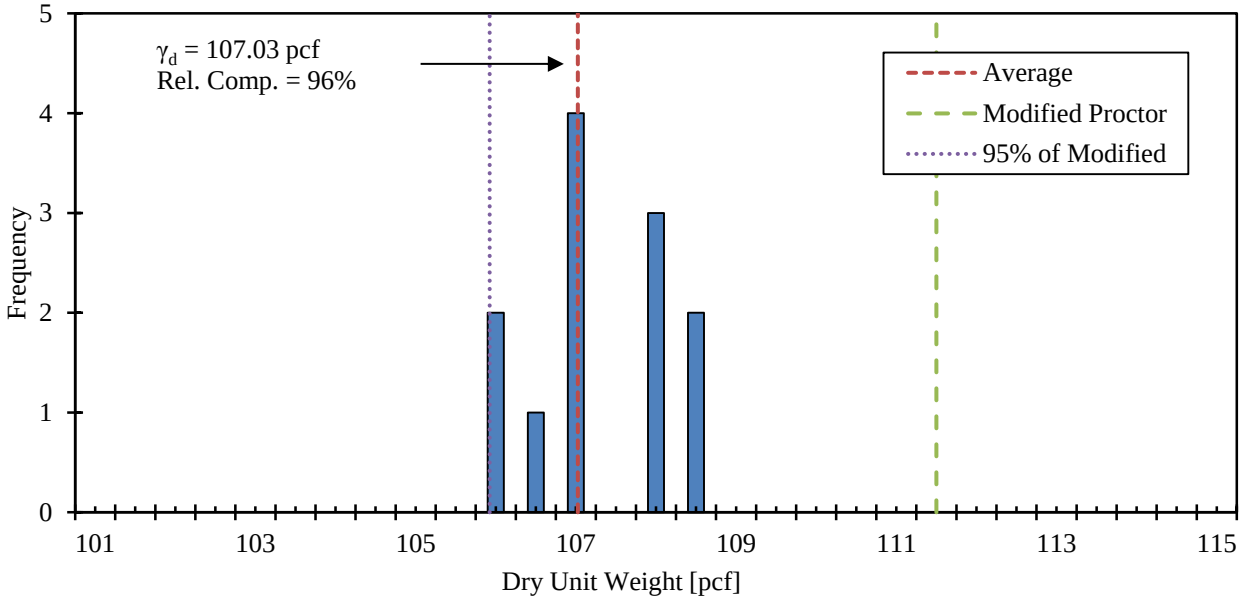

Figure 5. Backfill dry unit weight histogram for 0° skew test.

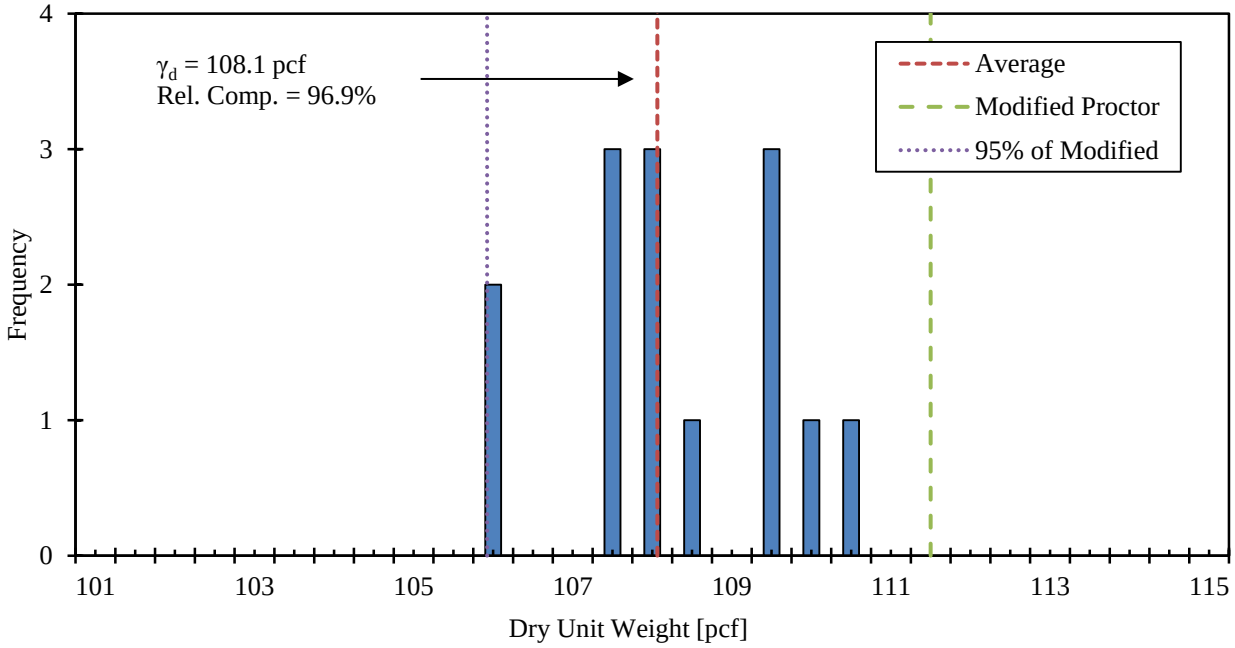

Figure 6. Backfill dry unit weight histogram for 15° skew test.

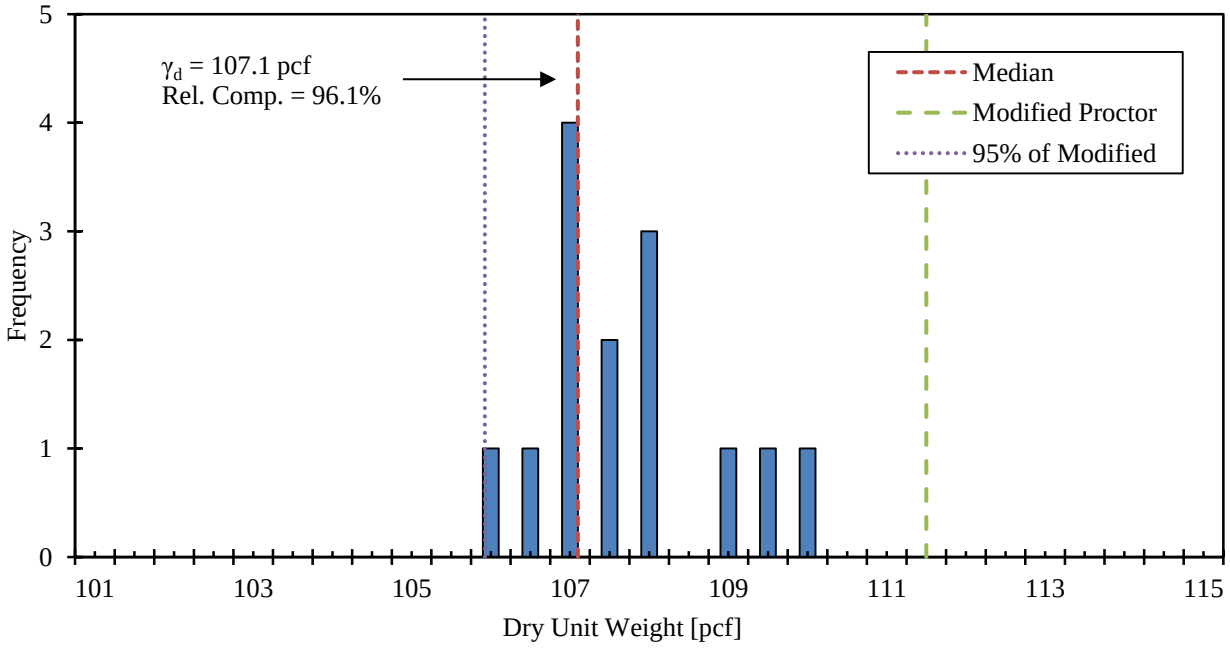

Figure 7. Backfill dry unit weight histogram for 30° skew test.

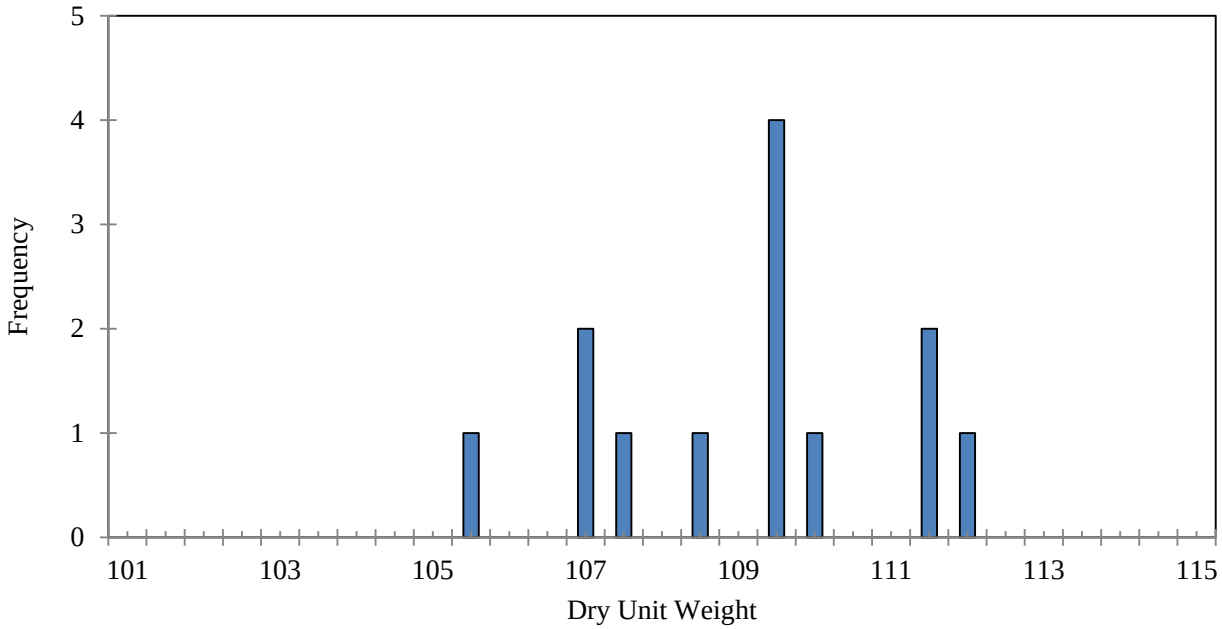

Figure 8. Backfill dry unit weight histogram for 45° skew test.

Moisture content measurements with depth below the pile cap surface are shown in Figure 9 through Figure 12.

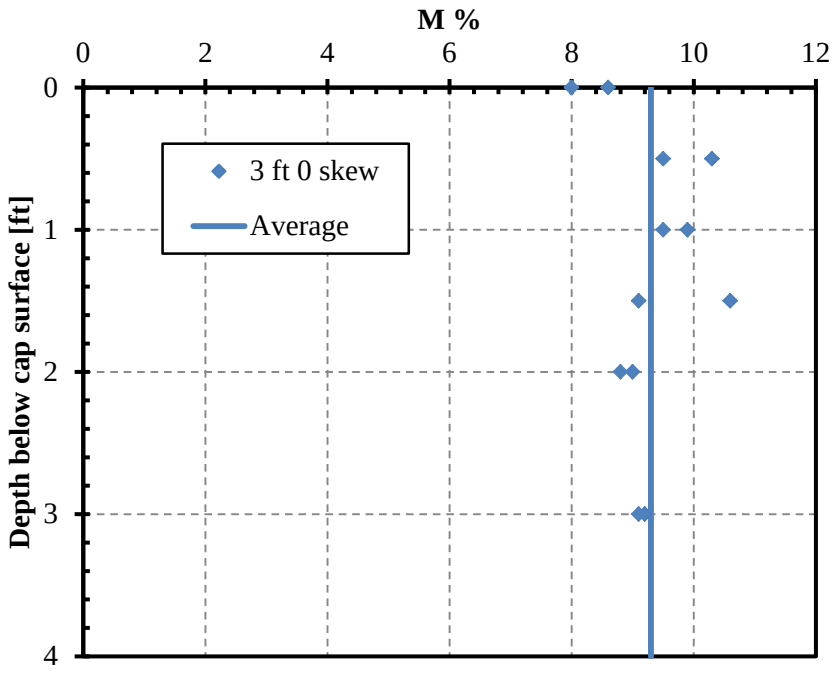

Figure 9. Moisture content measurements for 0° skew test.

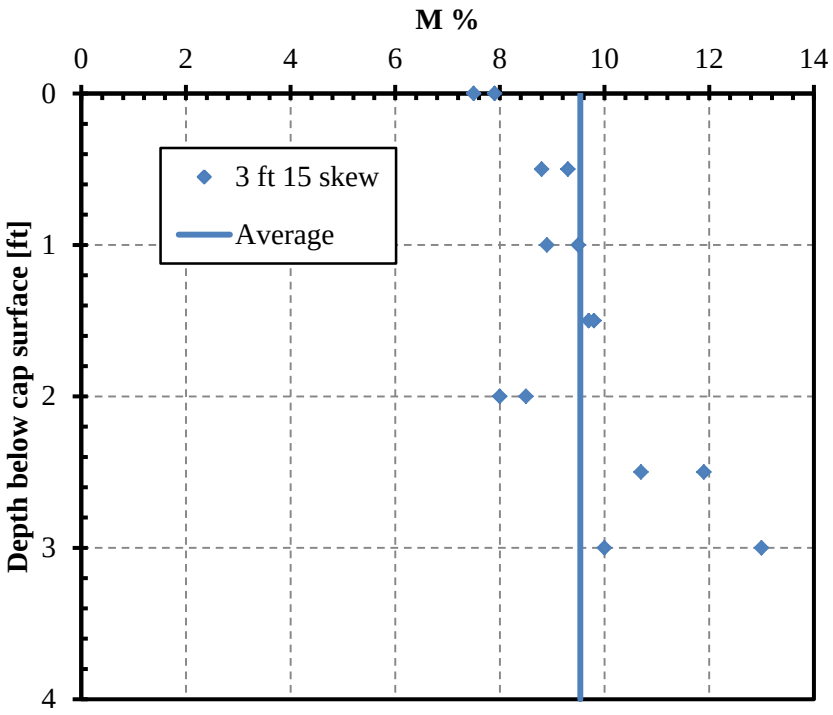

Figure 10. Moisture content measurements for 15° skew test.

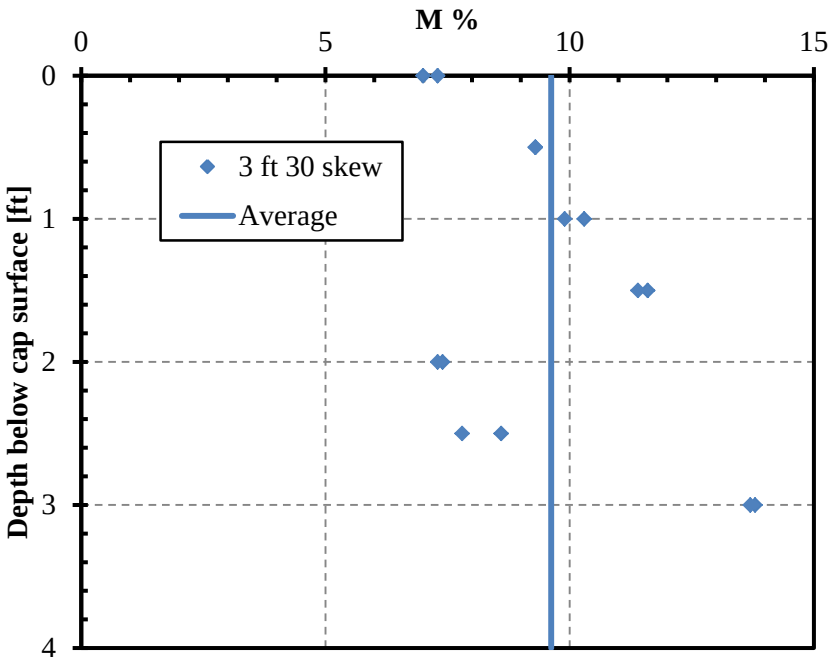

Figure 11. Moisture content measurements for 30° skew test.

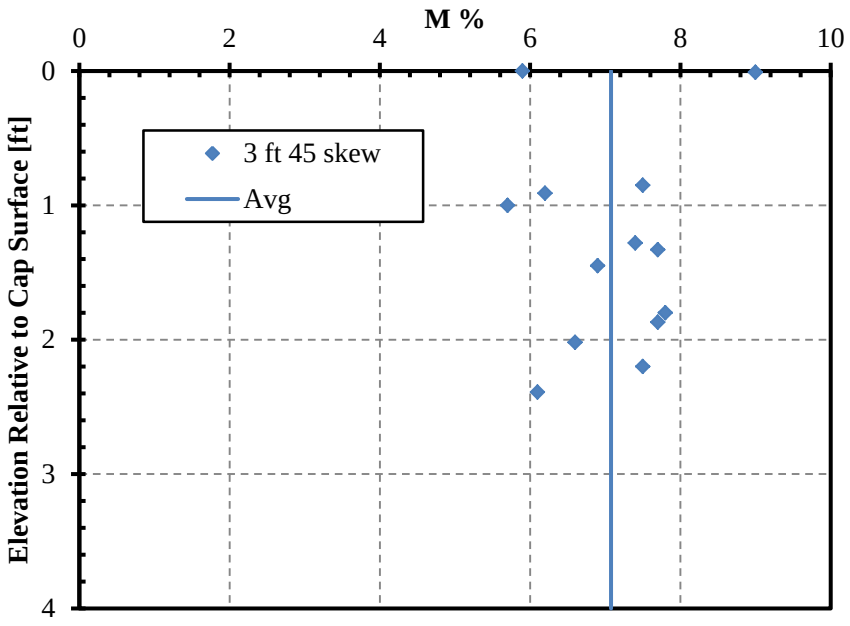

Figure 12. Moisture content measurements for 45° skew test.

Shear Strength

Direct shear tests were conducted at the field density and moisture content values, and the drained friction angle (ϕ') was found to be 41° with a cohesion of 96 lbs/ft^2 (4.61 kN/m^2). Previous researchers (Rollins and Cole 2006; Rollins and Jessee 2012) conducted direct shear tests and determined that the interface friction angle (δ) between similar sand and concrete was about 75% of the soil friction angle. For comparison purposes, the drained friction angle of the sand for the laboratory skew tests was 46° with a cohesion of 70 lbs/ft^2 (3.35 kPa) (Rollins and Jessee 2012).

General Test Procedures

Prior to testing with the backfill in place, a lateral load test was performed to determine the "baseline" resistance of the pile cap alone, and the pile cap with attached wedge. Because the pile cap had been previously employed for a number of tests, the baseline resistance has become relatively linear. Following the baseline test, backfill was compacted adjacent to the cap and a lateral load test was performed to obtain the total resistance. Following backfill compaction, the grid and soil columns were

installed and appropriate initial measurements, including relative elevations of the grid points, were recorded. The backfill material was completely excavated and recompacted for each individual test.

The pile cap (and attached wedge if applicable) was then pushed longitudinally into the backfill zone in 0.25-in (6.35-mm) increments at a velocity of 0.25 in/min (6.35 mm/min) to a final displacement of 3.25 in to 3.50 in (8.30 cm to 9.53 cm) using the two hydraulic actuators. At each 0.25-in (6.35-mm) displacement increment the load was held for approximately 2 minutes to observe the reduction in longitudinal force against the backwall as a function of time. On average, the reduction in force after 2 minutes was 7.6%.

A plot of the total load and corresponding baseline curve for the 0° skew test is shown in Figure 13. The resistance of the pile cap in the longitudinal direction is made up of both the passive and shear resistance of the pile cap. This resistance is represented by the difference between the total and baseline curves.

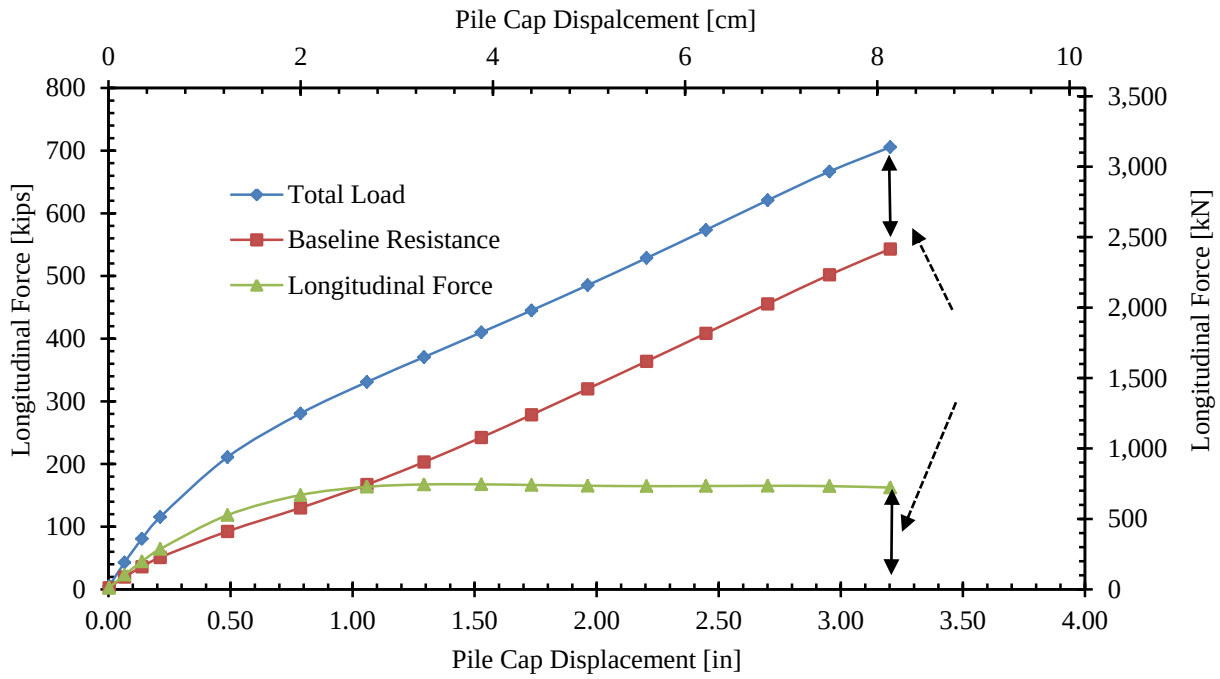

Figure 13. Total load, baseline resistance, and longitudinal force curves for 0° skew test.

TEST RESULTS

Failure Surface Geometry

Plots of the heave contours and surface cracks at the completion of the 0°, 15°, 30°, and 45° skew tests are shown in Figure 14 through Figure 17. It appears consistent in all four tests that maximum heave of the backfill soil occurs near the corners of the pile cap. Maximum heave for the 0° skew case was measured to be 2.4 in (70 mm), approximately 6.7% of the backfill height. Surface cracks radiated outward approximately 4 ft from both corners and another long crack was observed about 10 ft from the pile cap interface.

For the 15° skew case, a maximum heave of 1.9 in (48 mm) was measured, approximately 5.3% of the backfill height. More surface cracks were observed at the completion of the 15° skew test than the 0° test. It appeared that the entire failure wedge daylighted in a bulb pattern extending approximately 11 ft along the centerline from the pile cap face. Maximum heave for the 30° skew test was measured near the obtuse corner of the pile cap at 3.8 in (97 mm). This maximum heave was 10.6% of the backfill height, resulting in the largest amount of heave among all four tests. Surface cracks developed on the backfill very similarly to those in the 15° skew test. Maximum heave for the 45° skew test was measured near the acute corner of the pile cap at 2.4 in (70mm), the same value as the 0° skew test. The surface crack pattern again was very similar to the 15° and 30° tests, except the failure wedge daylighted at 12 ft from the pile cap face instead of 11 ft.

.

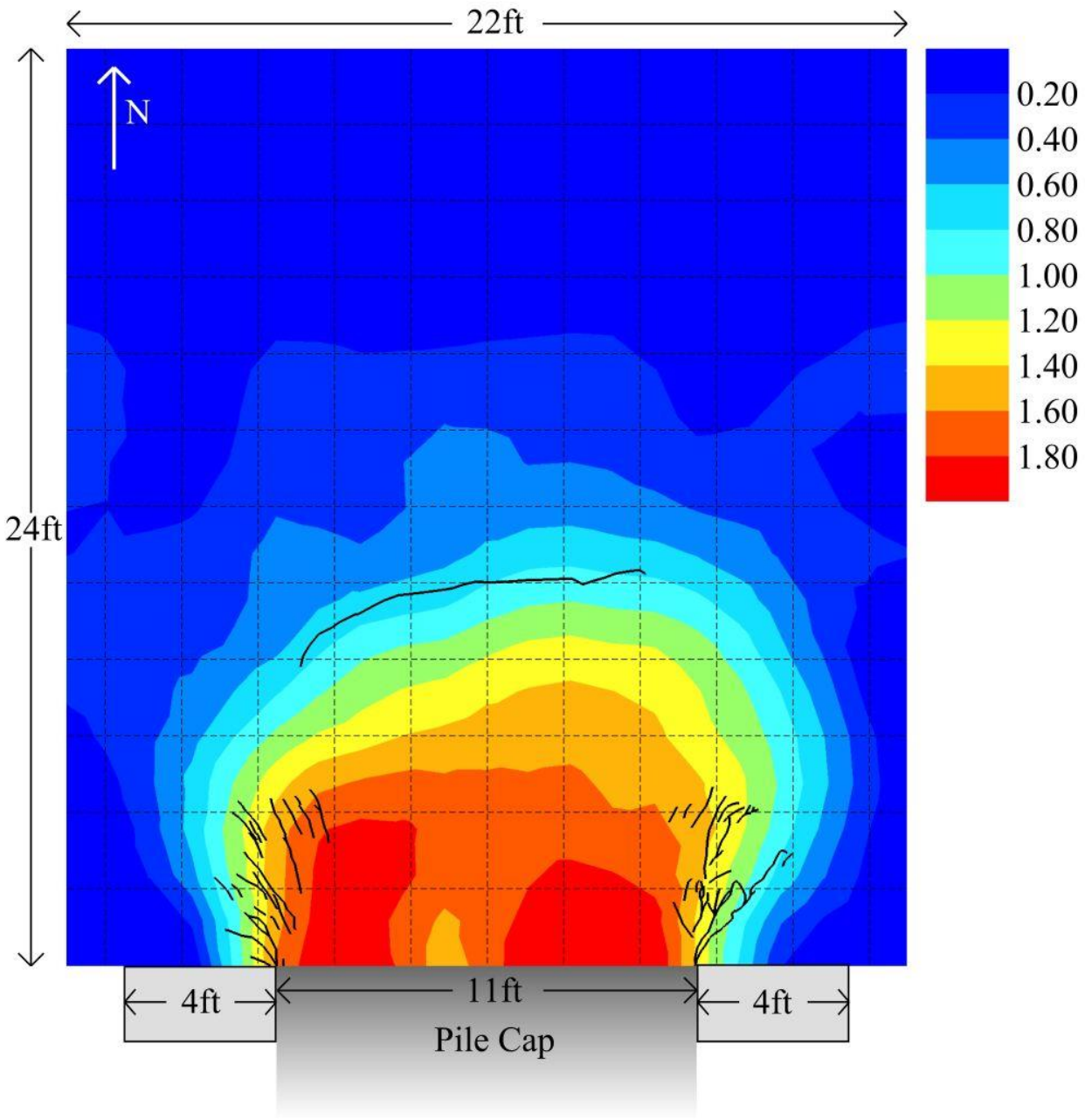

Figure 14. Heave contours (units in inches) and surface cracks at test completion for 0° skew test (NOTE: 1 inch = 2.54 centimeters).

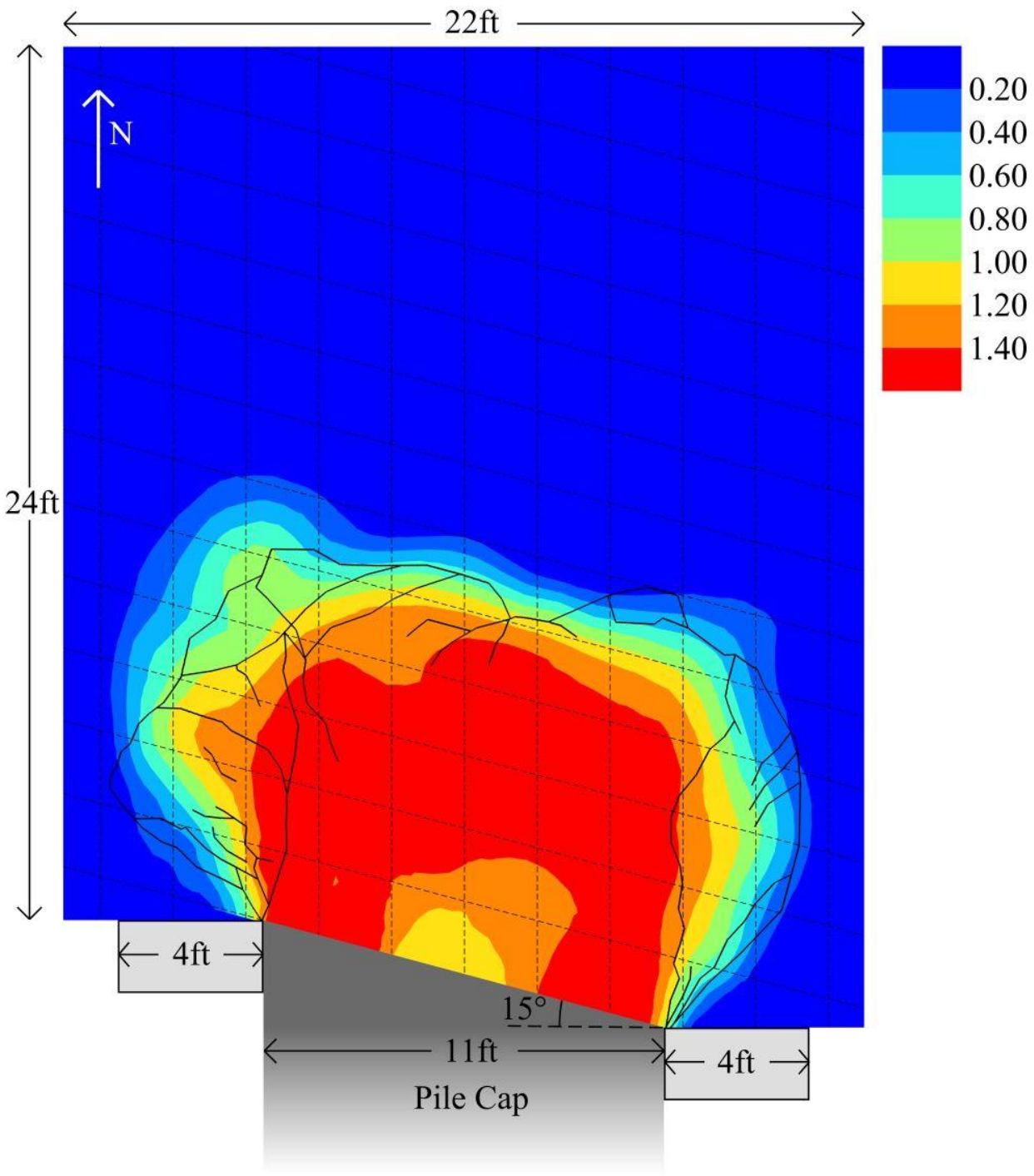

Figure 15. Heave contours (units in inches) and surface cracks at test completion for 15° skew (NOTE 1 inch = 2.54 centimeters)

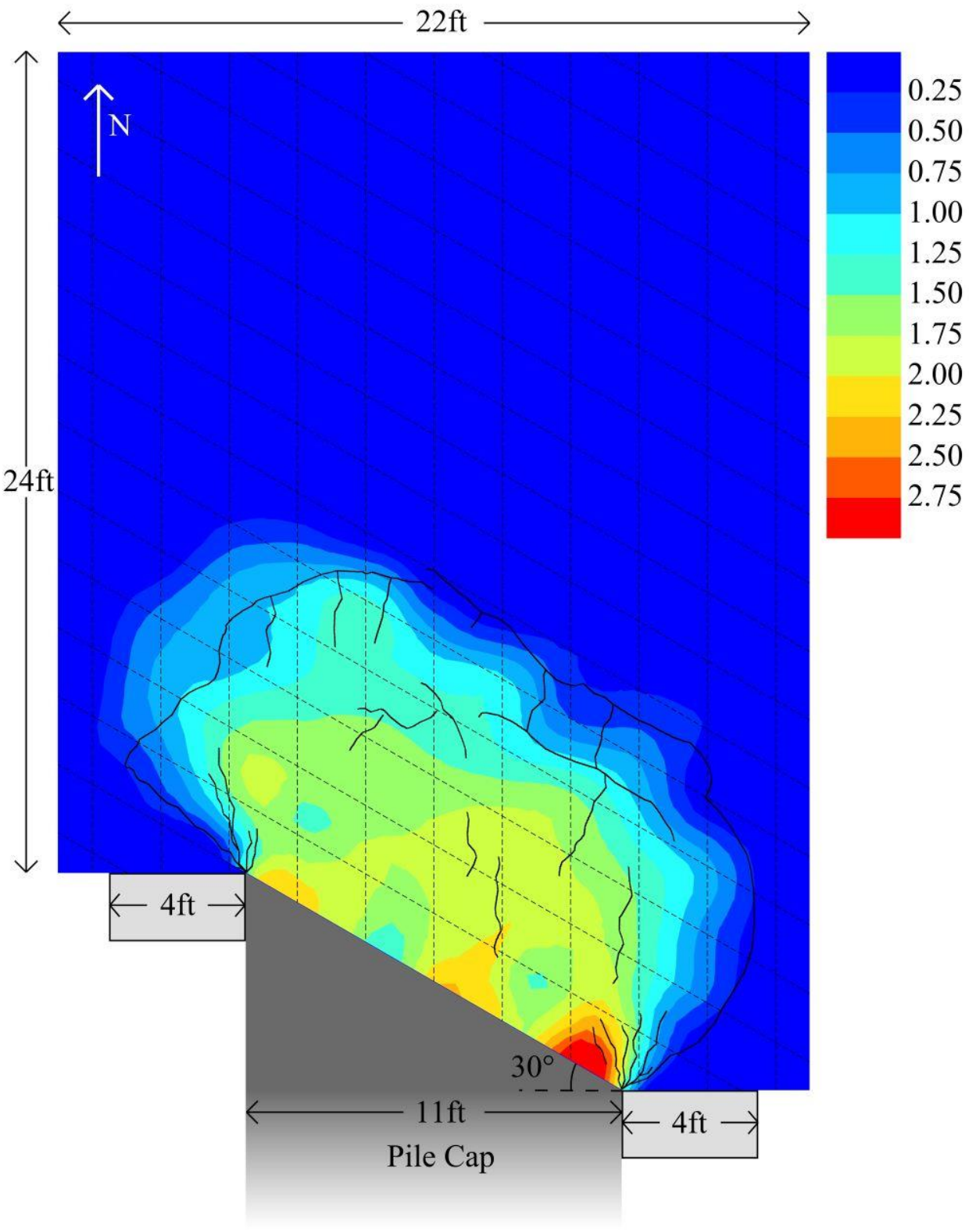

Figure 16. Heave contours (units in inches) and surface cracks at test completion for 30° skew (NOTE 1 inch = 2.54 centimeters)

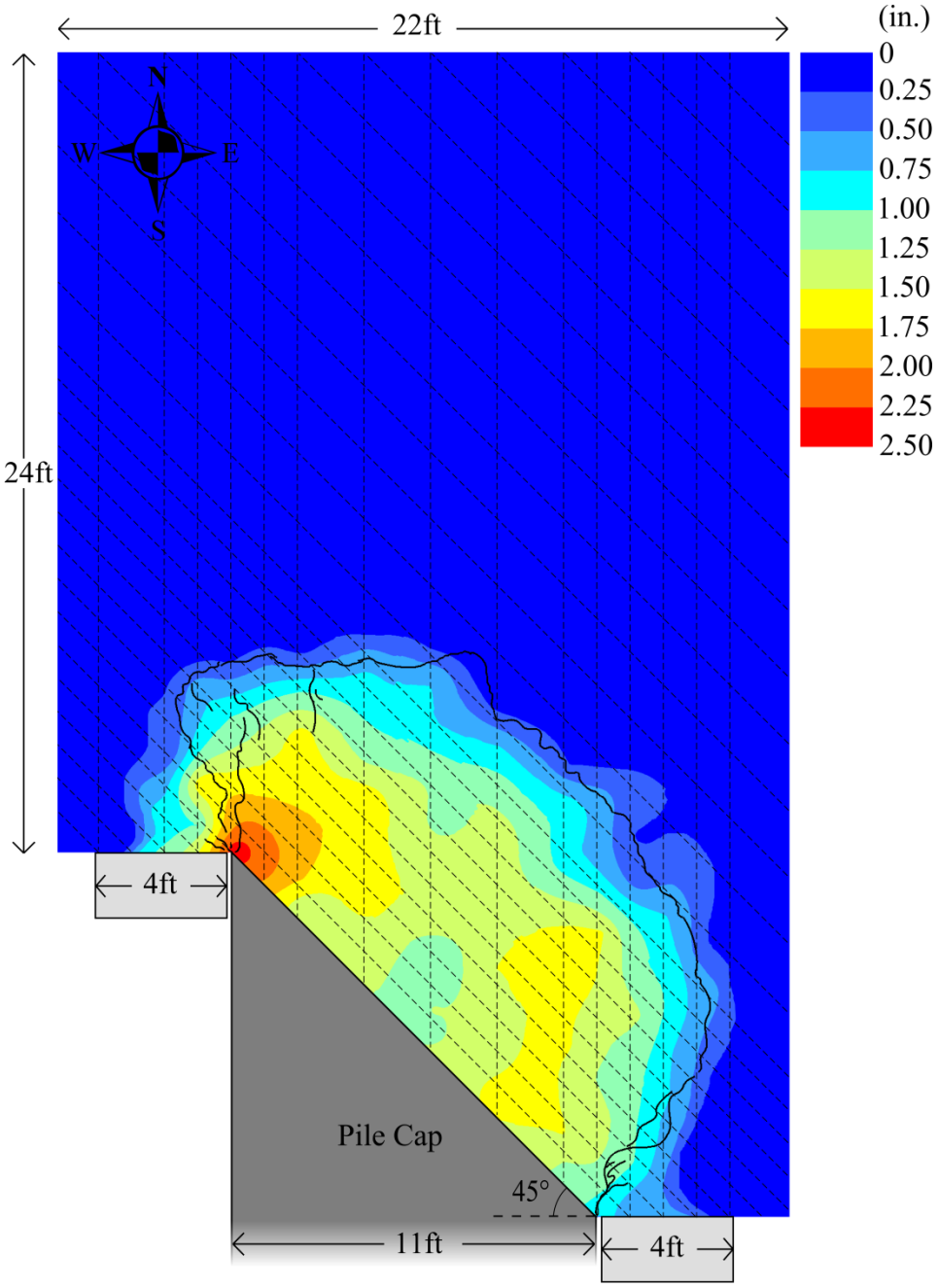

Figure 17. Heave contours (units in inches) and surface cracks at test completion for 45° skew (NOTE 1 inch = 2.54 centimeters)

Figure 18 illustrates the horizontal backfill soil displacement at the completion of the 45° skew test. The backfill generally displaced in the northeast direction at an average angle of 62° from horizontal.

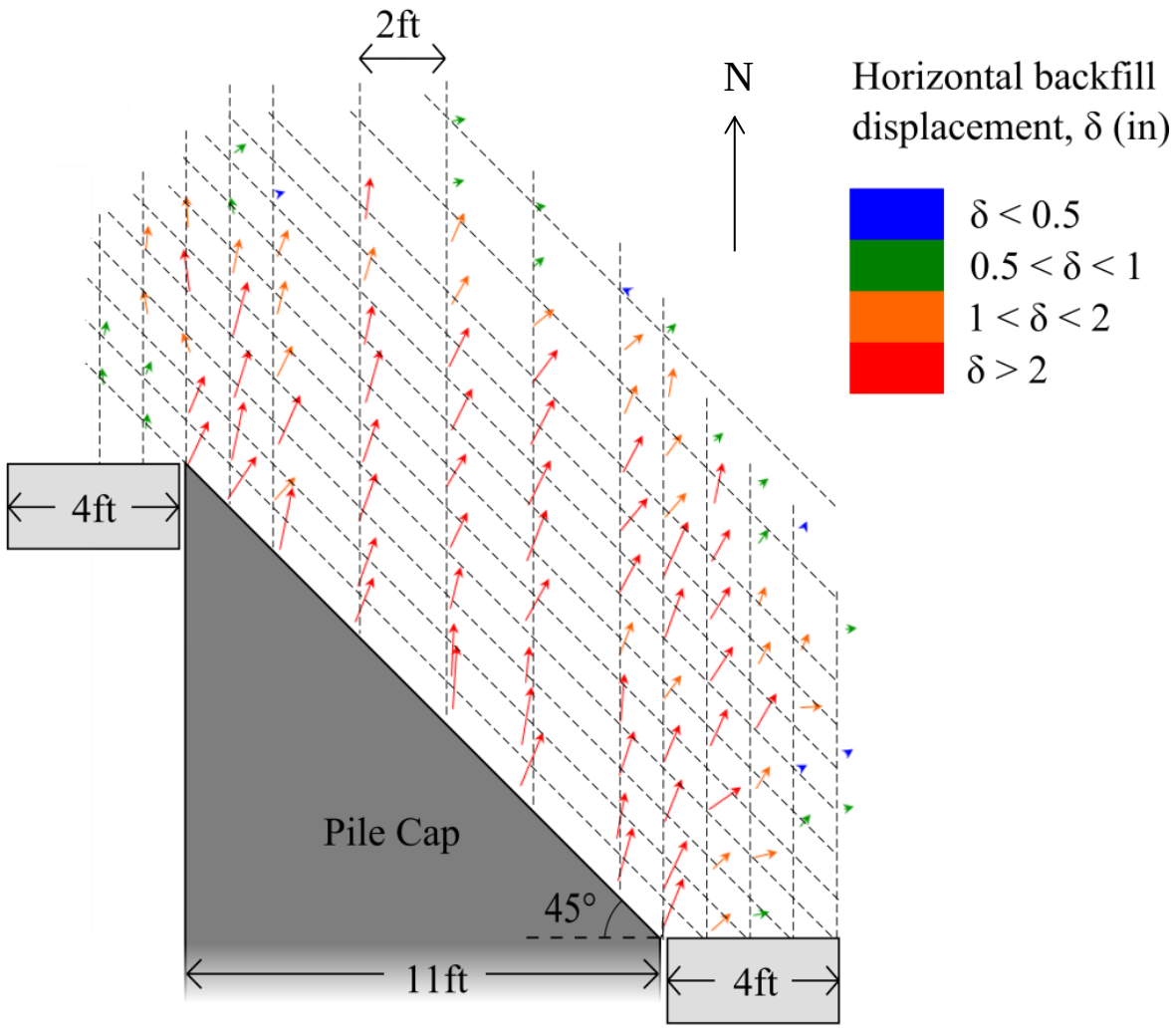

Figure 18. Soil displacement for 45° skew 3 ft. sand backfill unconfined.

Passive Force-Deflection Curves

Figure 19 shows the passive force vs. longitudinal deflection curves for the 0°, 15°, 30°, and 45° skew field tests. Passive force was calculated from the total actuator load corrected for the appropriate baseline curve using Equation (2). Backwall deflection was computed as the average deflection of the four string pots on the back of the pile cap. As shown in Figure 19 as the skew angle increases the peak passive force decreases. Nevertheless, for all four tests, the peak passive force was obtained at normalized deflections between 0.03H and 0.04H which is in good agreement with previous full-scale passive force

tests on dense backfill materials without any skew angle (Rollins and Cole 2006). For the 0° skew test the passive force-displacement curve remained essentially constant beyond the peak, while the passive force decreased about 20% for the 15° skew, 16% for the 30° skew, and. 40% for the 45° skew. The backfill for the 15° and 45° skew tests was somewhat denser than for the 0° skew test and thus somewhat more likely to dilate during shearing. Beyond the peak resistance, dilation would produce a lower density with reduced resistance.

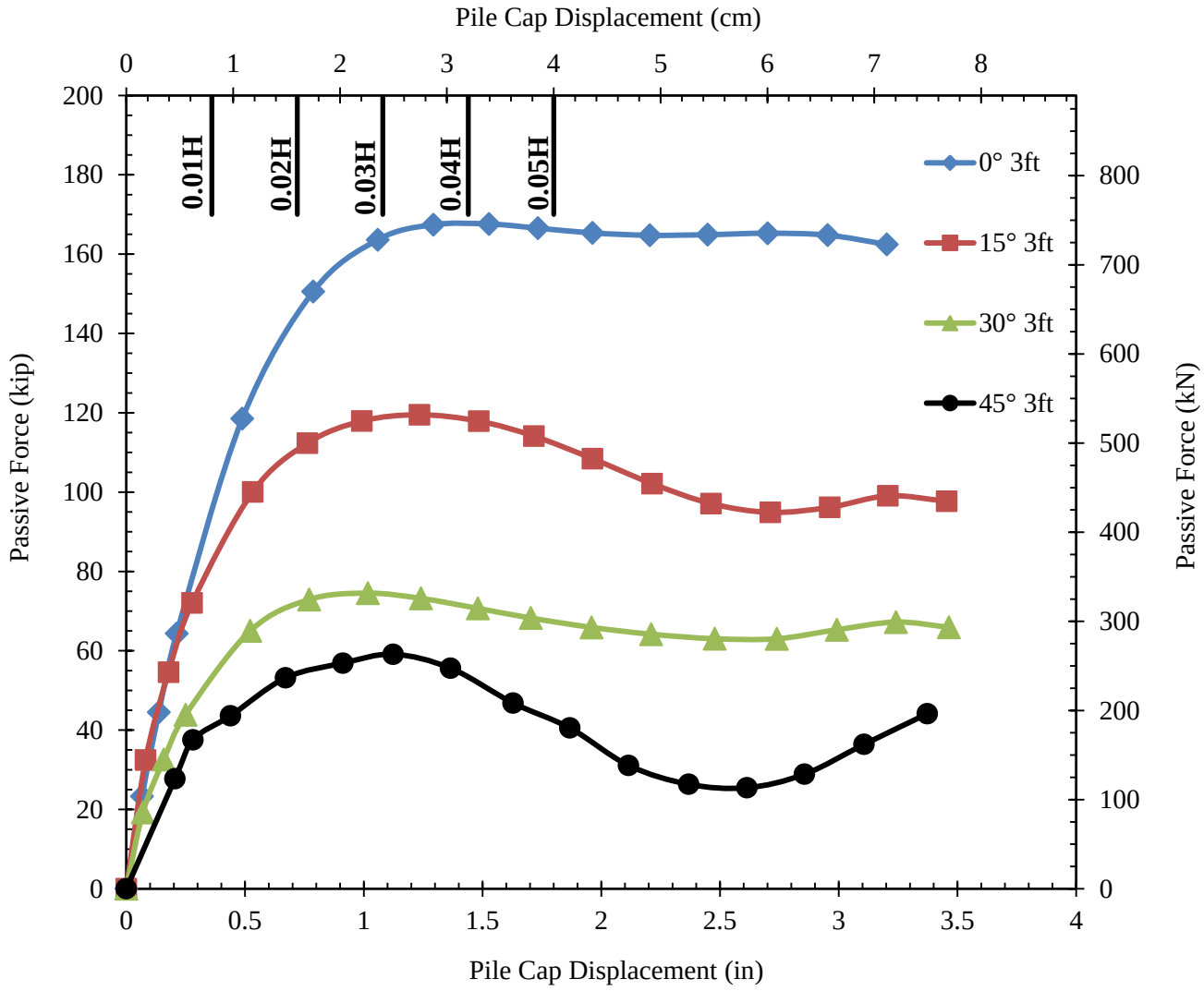

Figure 19. Passive force vs. deflection perpendicular to skew interface for 0°, 15°, 30° and 45° skews.

A comparison between the lab and field tests indicates that the passive force after normalization by the backwall width was higher for the lab tests. Because the lab tests were conducted so as to simulate plane-strain conditions, and the field tests used an unconfined geometry, the higher normalized passive force for the lab tests is not surprising because the friction angle is normally higher for plane strain conditions. Furthermore, the soil for the lab tests was compacted to a higher relative density. In addition to the higher normalized peak passive force for the lab tests, the peak passive force for the field tests developed at longitudinal deflections between 3% and 4% of the backwall height (H) whereas the plane-strain tests developed their peak passive force at deflections between 2% and 3% of H. The greater drop in passive force after the peak for the lab tests is consistent with the fact that the lab tests were compacted to a denser state and would therefore have had a greater tendency to dilate and experience a decrease in strength during shearing. The denser state may also explain the somewhat more brittle behavior for the lab tests as well.

Figure 20 plots the passive force reduction factor versus skew angle for the lab tests conducted by Rollins and Jessee (2012), for the numerical models reported by Shamsabadi et al. (2006), and for the results of this study. As can be seen from the Figure 20, Equation (1) predicts that at skew angles of 15°, 30°, and 45° the passive force reduction factors should be 75% ,53%, and 35% respectively, when compared to the 0° skew case. The measured reduction factors from the field tests were 71%, 44%, and 35% for the 15°, 30°, and 45° skew tests, respectively. The general agreement between the field test results and the numerical and lab test results suggests that 3D effects and backwall width to height ratios may have only a small effect on the reduction in passive force with respect to skew angle. These results support the notion that the equation for a reduction factor with respect to skew angle is generally applicable. However, results from additional large scale tests or computer analyses with different material properties and geometries would be desirable to further substantiate this contention.

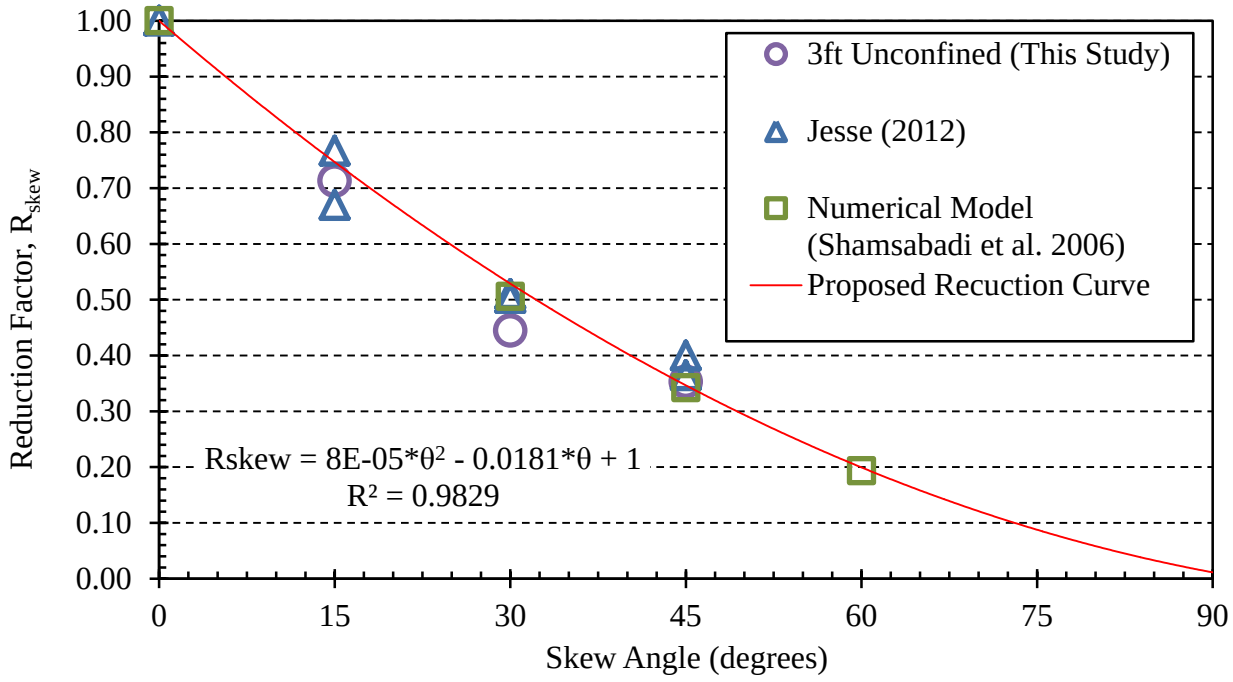

Figure 20. Reduction factor, R_{skew} (passive force for a given skew angle normalized by passive force with no skew) plotted versus skew angle based on lab tests (Rollins and Jessee 2012), numerical analyses (Shamsabadi et al. 2006) and s results from field tests in this study.

Pile Cap Displacement vs. Depth

Figure 21 through Figure 24 provide longitudinal deflection versus depth profiles obtained from both an inclinometer and a shape accelerometer array for the 0º, 15°, 30°, and 45° skew tests. The profiles shown below represent pile cap behavior for the final longitudinal displacement of the test. The depths are referenced to the top of the cap. The average deflection measured by the string pots at two elevations on the pile cap are also shown on these profiles for comparison purposes. The graphs demonstrate that the deflection measurements for the three systems were reasonably accurate and aligned with each other. The percent difference between the inclinometer and shape array profiles from the top of the cap to a depth of 20 ft (6 m) ranges between 0.01 and 1.0% for the 0° skew and between 0.01 and 1.8% for the 30° skew test. The 45° skew error ranged from 1.8 to 7.5% from depths 0 to 15 ft and reached 14% at about 17ft of depth. The increased disagreement is likely due to a testing error which

prevented accurate initial inclinometer readings for this test. The displacements below a depth of 20 ft (6 m), and below 18 ft for the 45° skew test, are very small and the error values in this zone are not particularly meaningful. Similar good agreement was obtained between the shape array and inclinometer for the other tests.

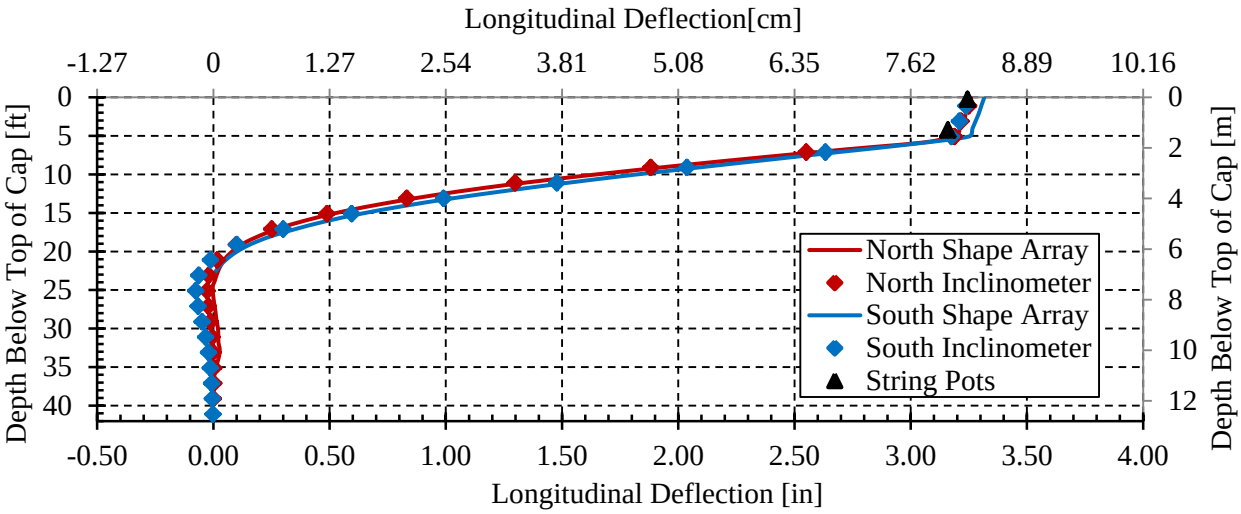

Figure 21. North and south 3-ft backfill 0° skew final deflection; comparing inclinometer, shape array, and string potentiometers.

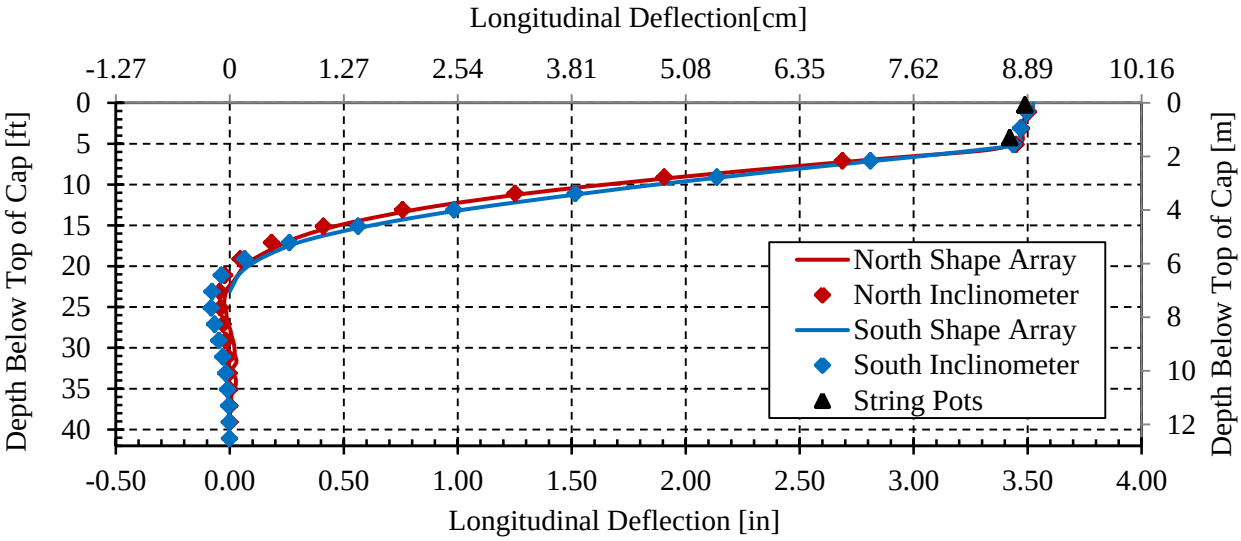

Figure 22. North and south 3-ft backfill 15° skew final deflection; comparing inclinometer, shape array, and string potentiometers.

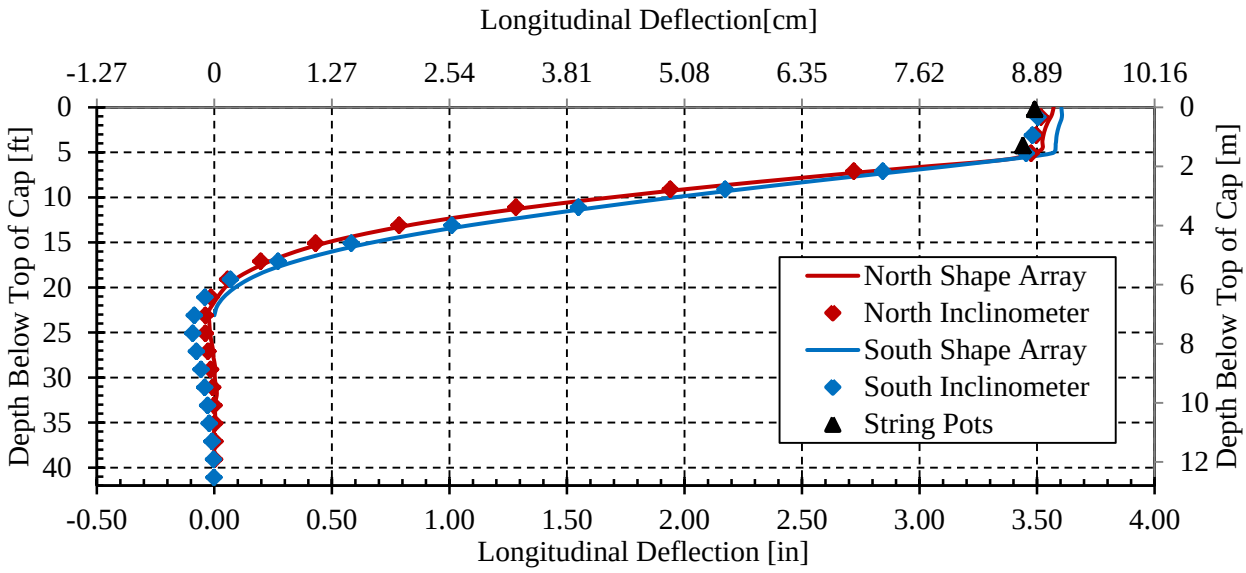

Figure 23. North and south 3-ft backfill 30° skew final deflection; comparing inclinometer, shape array, and string potentiometers.

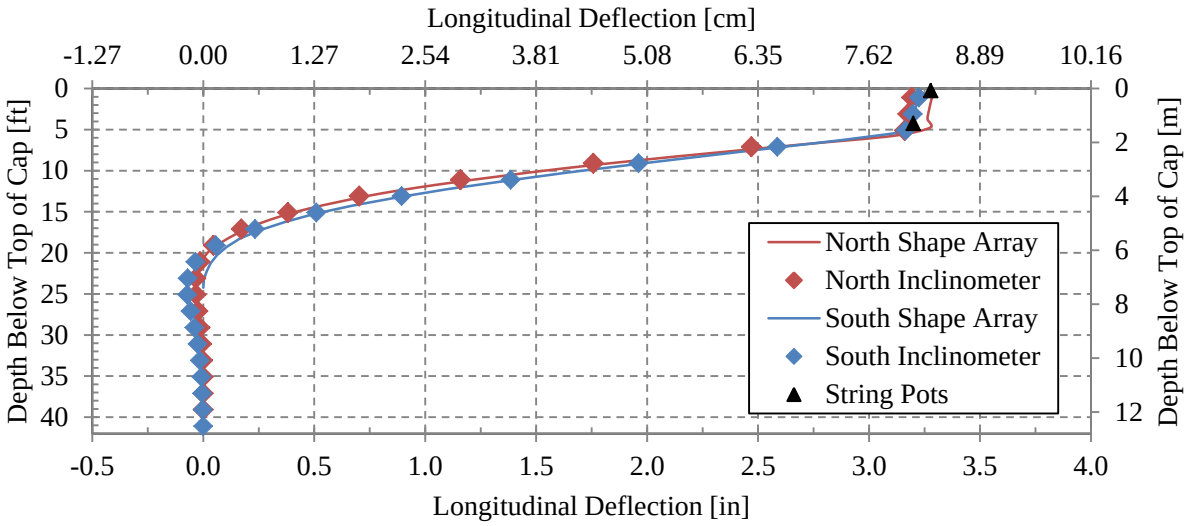

Figure 24. North and south 3-ft backfill 45° skew final deflection; comparing inclinometer, shape array, and string potentiometers.

The measurements indicate a relatively linear deflection profile within the pile cap and small cap rotations. Below the base of the cap, the piles deflect in a non-linear fashion with the deflections reaching

a point of counterflexture at depth of approximately 21 ft (6.3 m) and a point of fixity at about 31 ft (9.45 m). Agreement between the north and south inclinometers was generally very good.

Transverse deflection versus depth profiles for the pile cap in each test, recorded by shape arrays and inclinometer, are plotted in Figure 25 through Figure 28. Plotted on a smaller scale, the percent error seems larger than the longitudinal error although the magnitude difference is small. However, as observed for the deflections below 20 ft (6.1 m) in the longitudinal test, the percent difference is exaggerated due to the smaller scale. The percent difference is within the error thresholds of each instrument (±1.5 mm/30 m for shape array, and ±1.24 mm/30m for inclinometer (Rollins et al. 2009). Results are similar for the tests for the 15° and 30° skew angles. The 45° skew test shows significant transverse error, which could be attributed in part to the lack of initial readings for this test as previously mentioned. However, other tests from this testing period showed similar transverse disagreement from depths of 6 ft (1.8 m) to 20 ft (6.1 m), suggesting that the shape array was perhaps twisted along those depths. The maximum disagreement for this test is about 0.7 in (17.8 mm). For all tests, once again, the shape of the deflection profile indicates essentially linear deflection in the pile cap and very small rotations. The deflection in the piles is non-linear and decreases to zero at a deflection of about 20 ft (6 m).

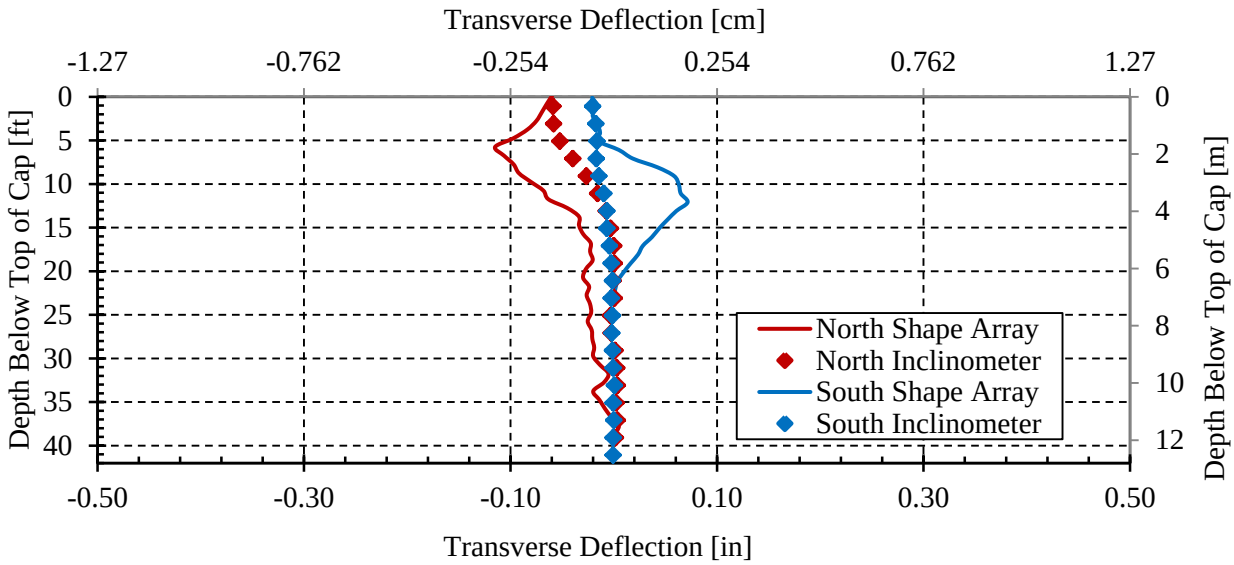

Figure 25. North 3-ft backfill 0° skew final deflections; comparing inclinometer and shape array.

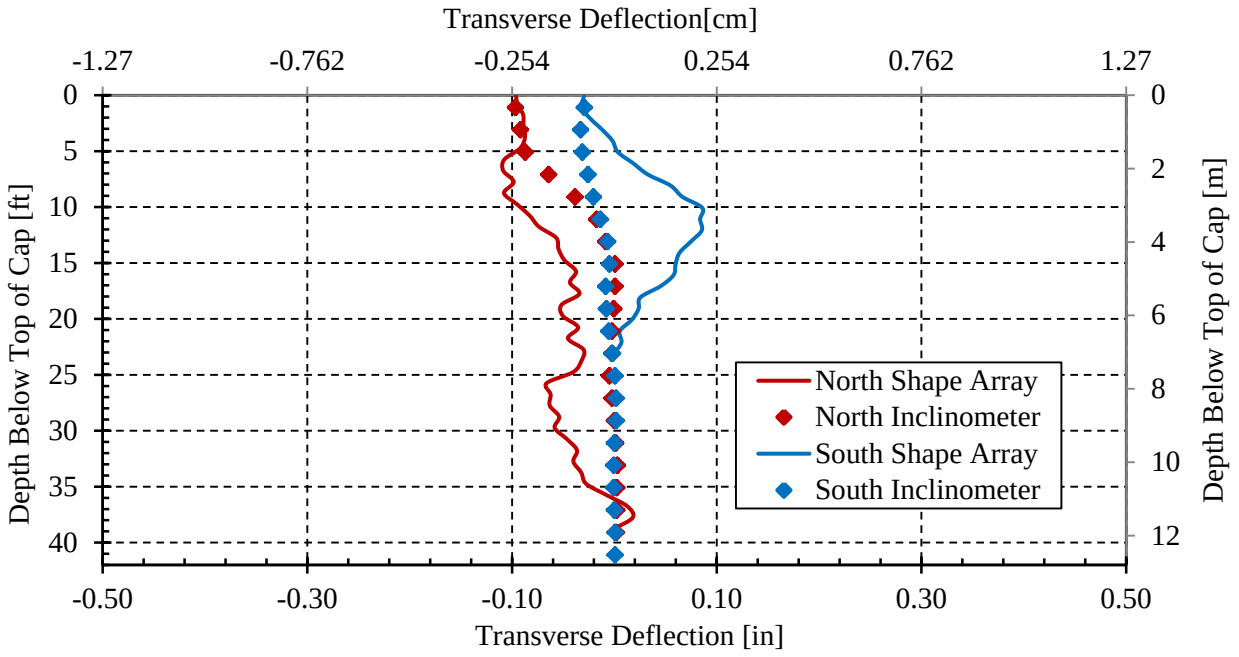

Figure 26. North 3-ft backfill 15° skew final deflections; comparing inclinometer and shape array.

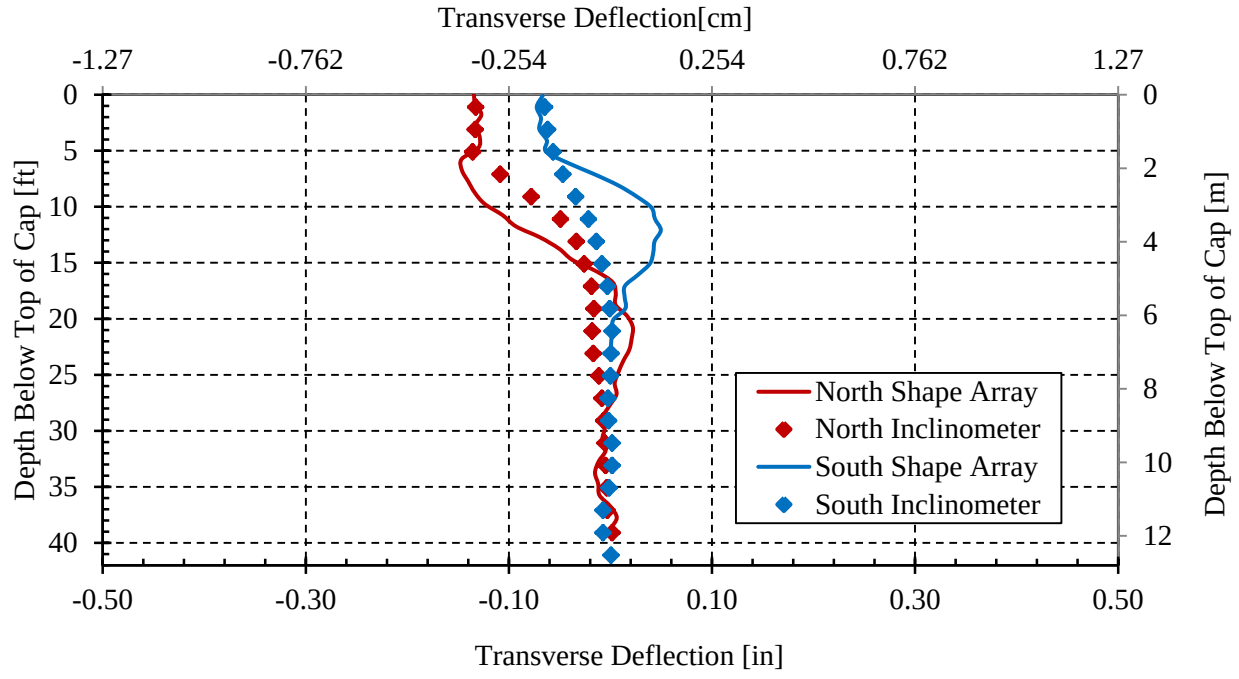

Figure 27. North 3-ft backfill 30° skew final deflections; comparing inclinometer and shape array.

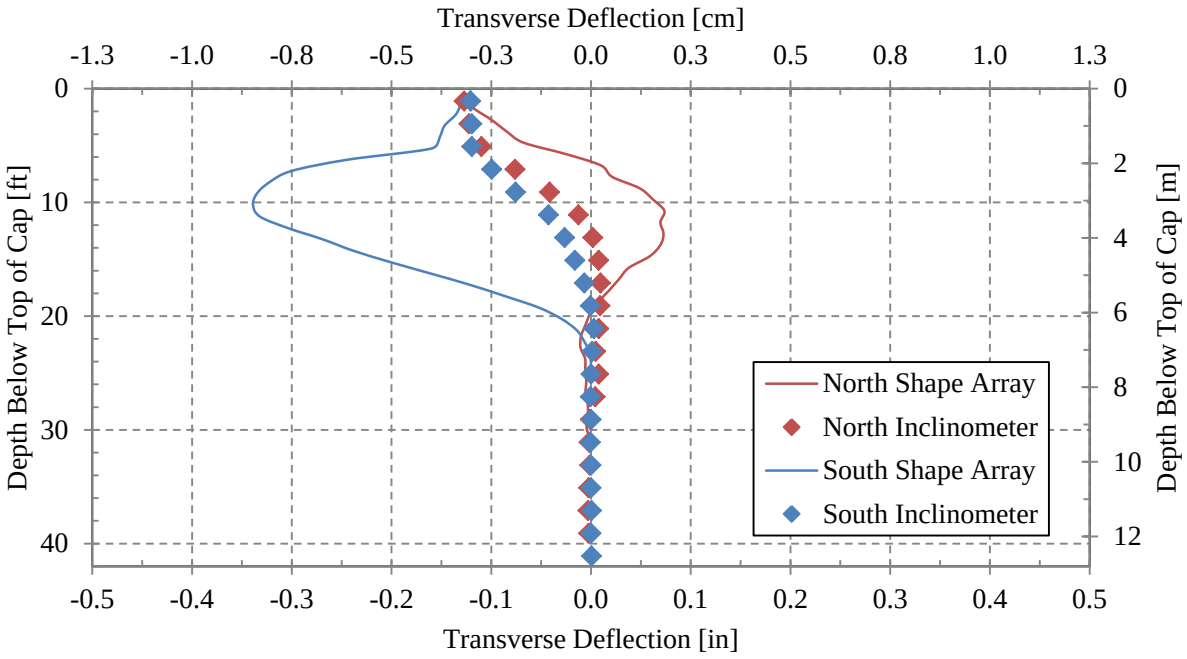

Figure 28. North 3-ft backfill 45° skew final deflections; comparing inclinometer and shape array.

Although the inclinometer readings were only taken at the maximum deflection for each load test, shape array profiles in the longitudinal and transverse directions were obtained at each deflection increment for each test. For example, Figure 29 shows profiles of longitudinal deflection vs. depth for each deflection increment for the 0° skew test. The 15°, 30°, and 45° skew test profiles are shown in Figure 30 through Figure 32. As the deflection level increases the deflection of the pile cap remains linear but the rotation progressively increases while the depth to the point of fixity increases. Similar curves were obtained in the transverse direction. At smaller deflection levels there are some variations associated with the small measurement errors; however at larger deflections, the data was accurate and useful in visualizing the pile movement.

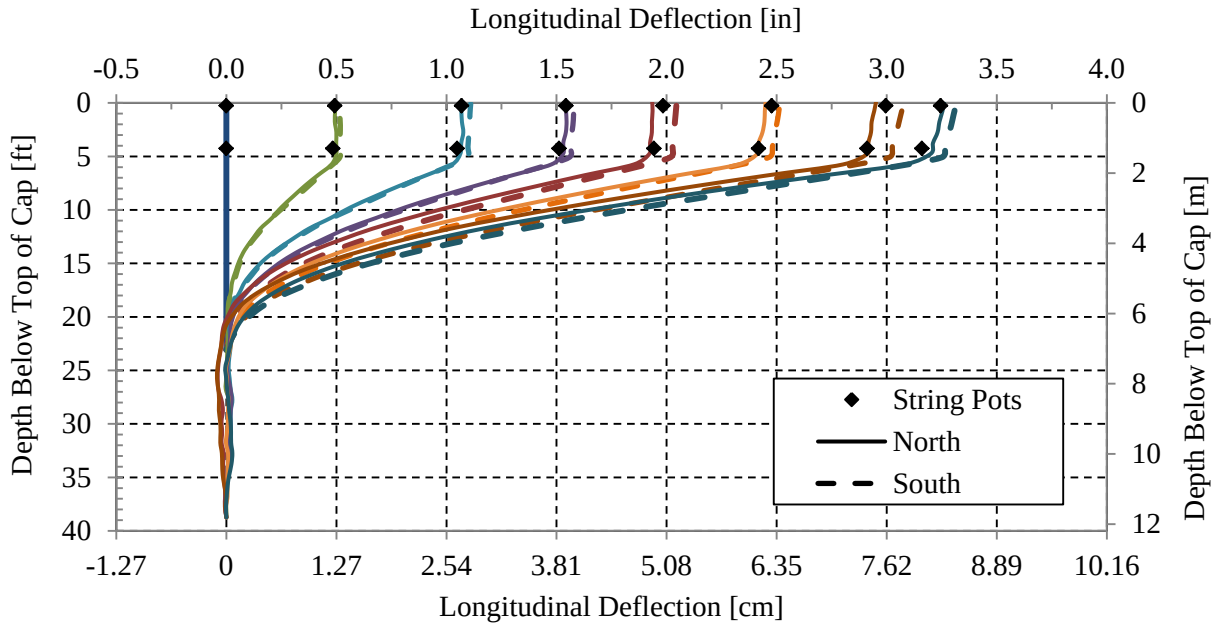

Figure 29. Longitudinal deflection vs. depth curves from north and south SAA data at various deflection increments for 0° skew test.

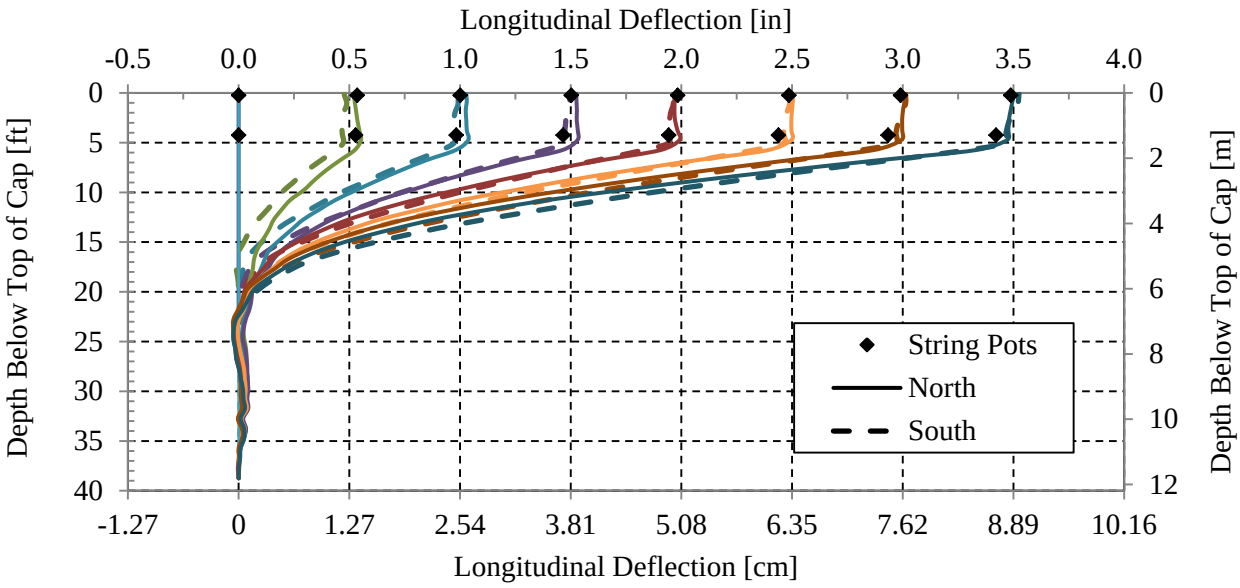

Figure 30. Longitudinal deflection vs. depth curves from north and south SAA data at various deflection increments for 15° skew test.

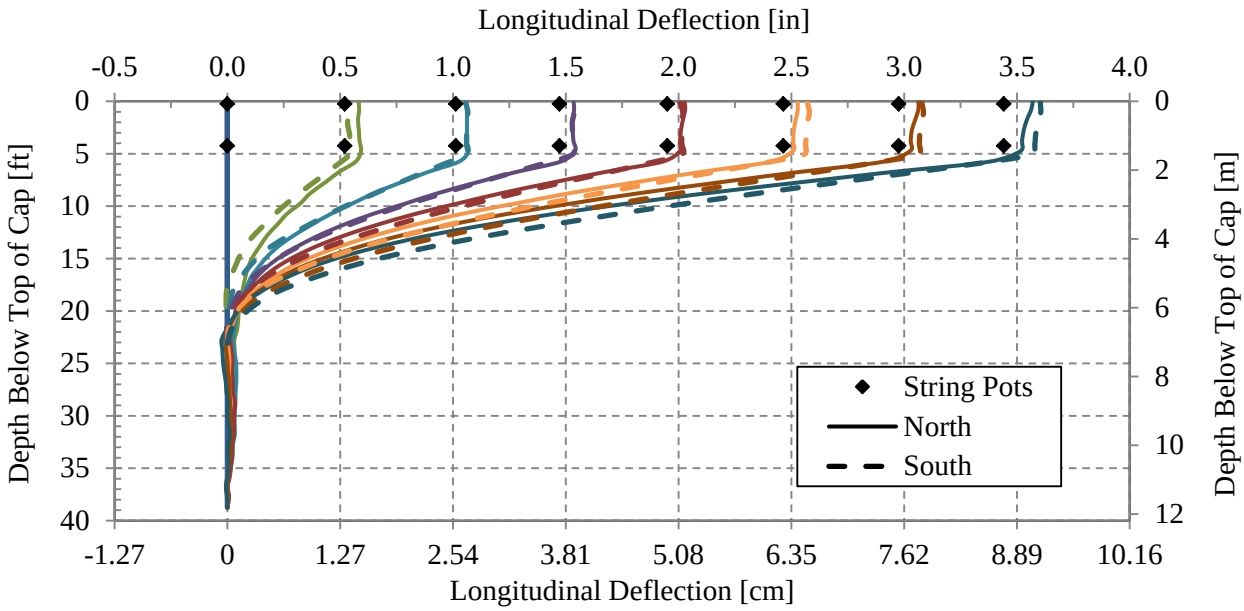

Figure 31. Longitudinal deflection vs. depth curves from north and south SAA data at various deflection increments for 30° skew test.

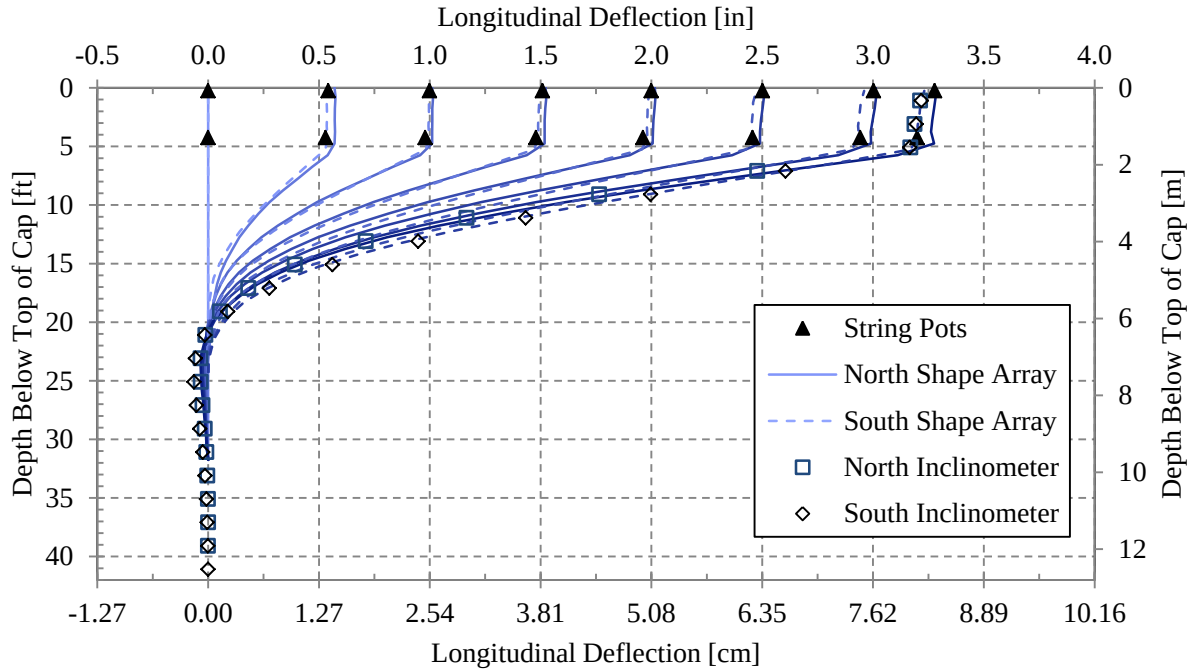

Figure 32. Longitudinal deflection vs. depth curves from north and south SAA, inclinometer, and string pot data at various deflection increments for 45° skew test.

As noted previously, the inclinometer and shape arrays measured transverse deflections for the north and south sides of the pile cap with depth. The measured transverse deflections at the top of pile cap on both the north and south sides of the cap after the last deflection increment for each test are plotted in Figure 33 from a plan view perspective. By connecting these points on the north and south sides, the rotation of the cap can be visualized as shown in Figure 33. Although deflections of both actuators were kept relatively consistent throughout the test to displace the cap longitudinally, rotation and transverse deflection still occurred. For the 0°, 15°, 30° and 45° skew tests, the pile cap ultimately shifted to the west (in the direction of the skew) by 0.04, 0.07, 0.10 and 0.13 inch, respectively. Thus, the transverse displacement progressively increased as the skew angle increased. In all cases, the pile cap ultimately rotated counterclockwise with rotations of 0.02°, 0.03°, 0.05and 0.003° for the 0°, 15°, 30° and 45° skew tests, respectively. Therefore, rotations were small and relatively unaffected by skew angle.

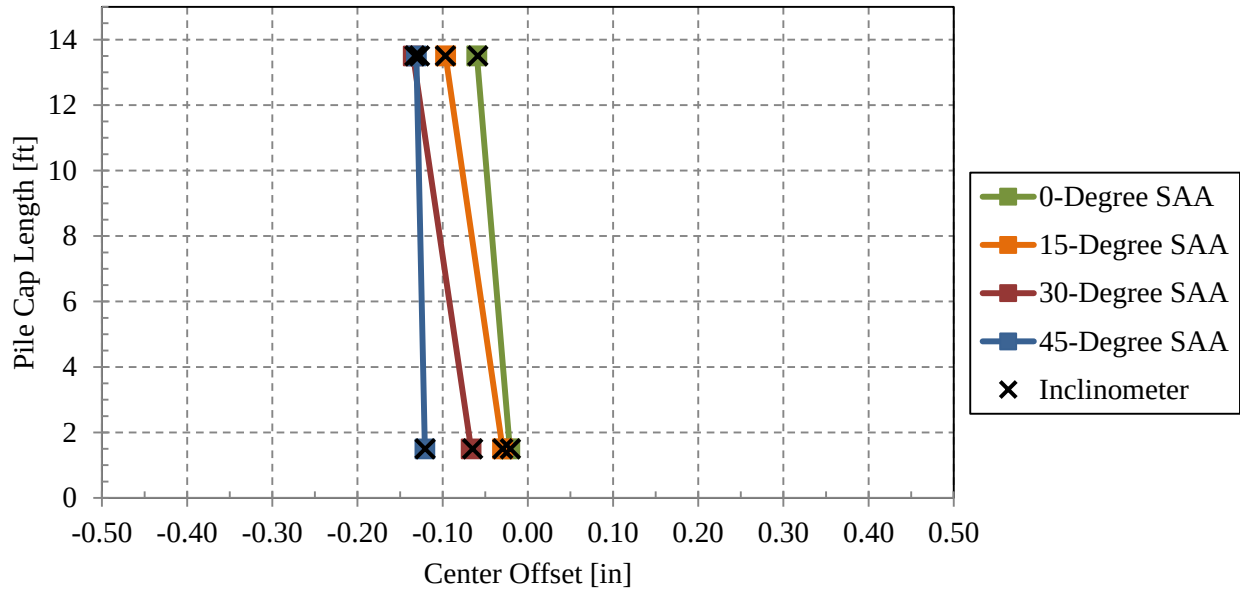

Figure 33. Transverse pile cap deflection and rotation determined between north and south shape array and inclinometer data

Pressure Distribution

As indicated previously, a total of six "Fat Back" pressure cells were installed horizontally across the face of the 30° skew wedge, as shown in Figure 34 (a). This instrumentation detected horizontal pressure shifts within the soil as the pile cap moved forward. Unfortunately, pressure plate PP1498 failed to function properly during the first test due to difficulties while removing the concrete form. However, the remaining five pressure plates still produced sufficient data to provide understanding of pressure distribution changes that occurred. All figures regarding pressure distribution within this chapter will be presented from the standpoint of the plan view shown in Figure 32 (b).

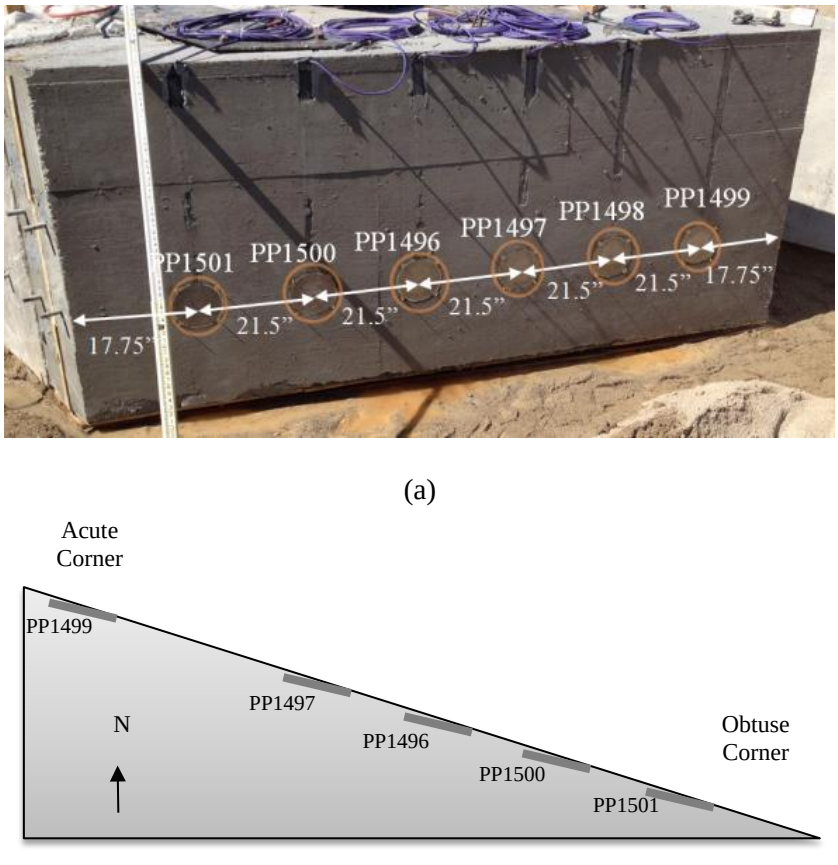

Figure 34. (a) Pile cap wedge interface (b) plan view drawing of pressure plates.

For the 30° skew, results revealed the pressure to be relatively uniform for the first inch (2.54 cm) of displacement, as seen in Figure 35 (a). The pressure then shifted in Figure 35 (b) to the obtuse end of the pile cap and dropped along the middle portion of the wall. At the displacement of 1.5 in (3.81 cm) shown in Figure 35 (c), the passive force reached a maximum pressure and the soil theoretically sheared, causing the pressure to suddenly shift more towards the obtuse end of the pile cap. This distribution corresponds to findings by Apirakyorapinit et al. (2012) which explain that stresses on bridge girders are highest on the obtuse side where the girders are being pushed into the backfill.

As the cap continued to move longitudinally, the overall pressure of the sheared soil and backwall decreased, with the greatest drop being on the obtuse end (see Figure 35 (d)). The final distribution (longitudinal displacement of 3.5 in) had its highest pressures at a locations of 1.3 ft (0.40 m) 7.5 ft (2.29 m) from the acute corner and its lowest pressure in the center of the pile cap (see Figure 35 (e)). The complete pressure progression is provided in Figure 35 (e) for comparison purposes.

Referring to the distribution of maximum pressures found in Figure 35 (c), results from this test also coincide with findings obtained by Sandford and Elgaaly (1993) in that they found the pressure on the obtuse side of a fully functioning bridge abutment to be greater than on the acute side. The higher pressure that developed on the obtuse side of the wall was attributed to possible rotation of the abutment. However, pressure distributions from the 30° skew test in this study vary from Sandford and Elgaaly who assumed a linear pressure distribution based on two pressure measurements. This is most likely caused by 3D effects exerting an additional pressure on the acute corner of the wedge. However, elastic theory also predicts that the pressure at the corners of wall will be higher than near the center, as shown in Figure 36 (Hegger et al., 2007).

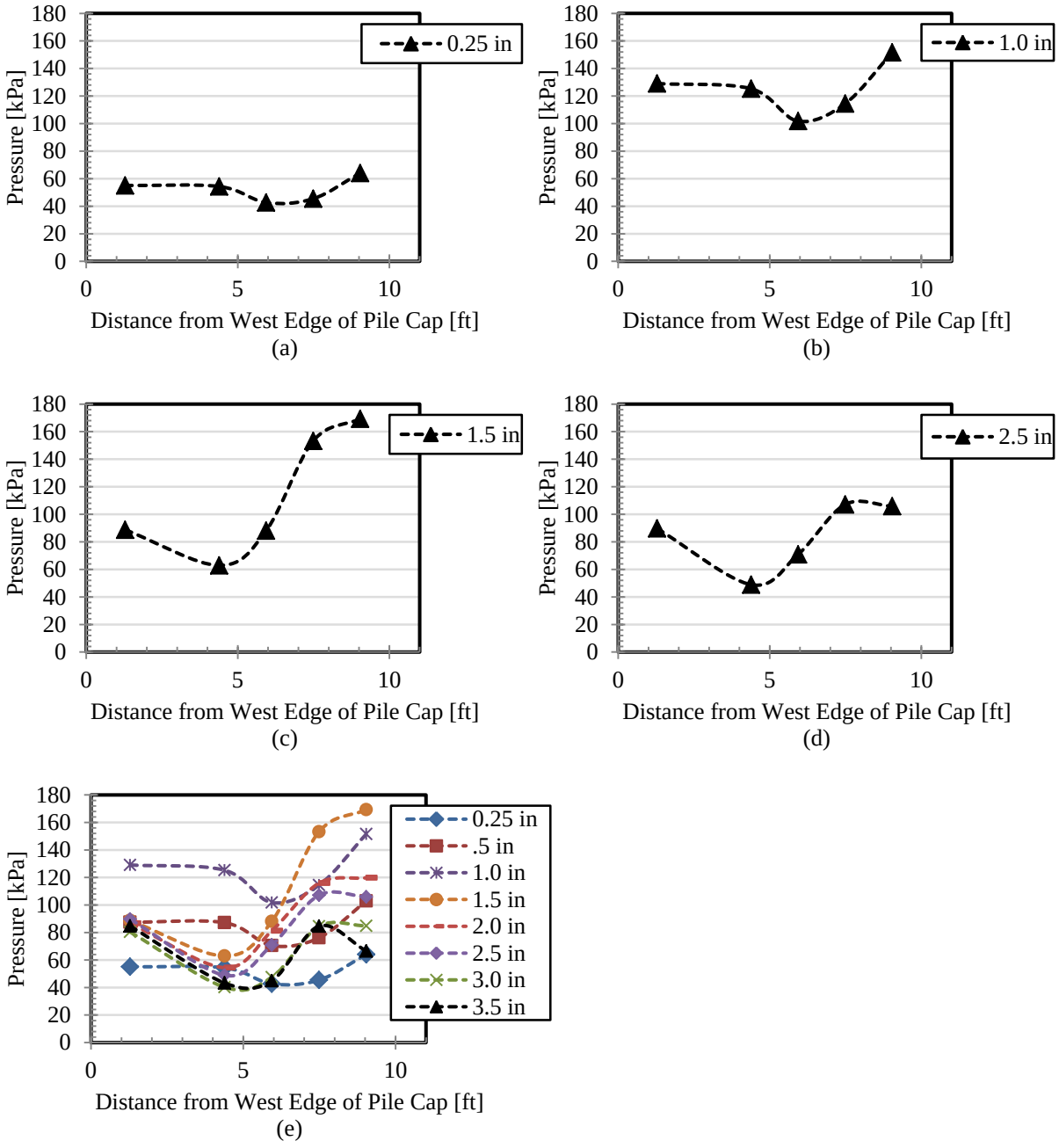

Figure 35. Progression of horizontal pressure distribution with pile cap movement.

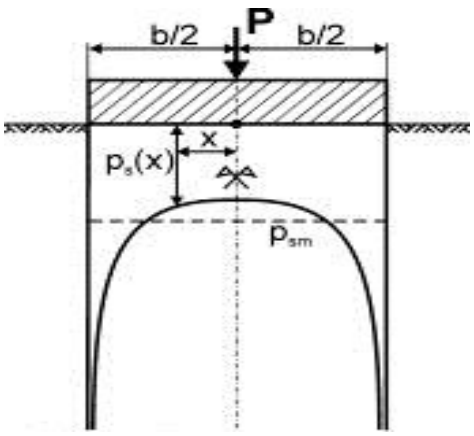

Figure 36. Soil pressure distribution under a rigid footing as shown by the elastic theory (Hegger et al., 2007).

Sandford and Elgaaly's study suggest a linear increase between the acute and obtuse corners. However, since no instrumentation was installed along the middle portion of the abutment interface in their study, it is possible that their backfill also experienced a similar decrease in pressure within the central portion of the soil distribution profile that was not accounted for because of the scarcity of instrumentation. By selecting pressure values from the 30° skew test a pressure distribution can be superimposed to fit the data points obtained in Sandford and Elgaaly's model, as shown in Figure 37 (b), which points out the possibility of alternate distributions occurring between Sandford and Elgaaly's two data points.

Since rotation about the longitudinal axis was extremely limited during the 30° skew test, it can be implied that rotation was not the only cause of the variance in pressure distribution along the soil-backwall interface. Higher pressures can still develop even when the pile cap is restrained as suggested by elastic theory. The non-linearity of these pressure distributions will likely magnify when rotation is incorporated because small variations in rotation of the pile cap could have pronounced effects on the pressure distribution.

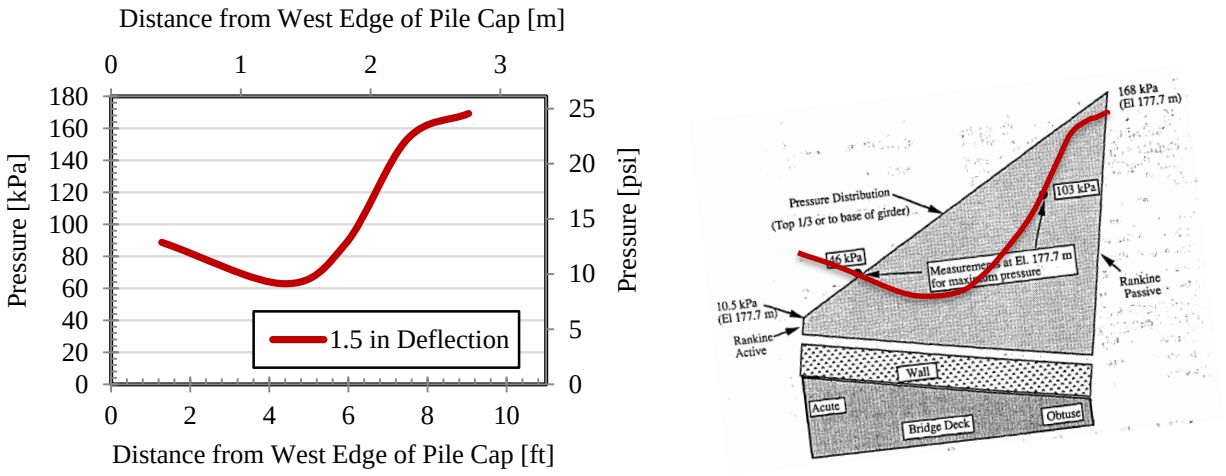

Figure 37. (a) Horizontal pressure distribution for the 30° test 1.5 in (3.81 cm) pile cap deflection, (b) horizontal pressure distribution superimposed onto Sandford and Elgaaly's model from Error! Reference source not found.**.**

The total pressure detected by the pressure plates was converted to a force magnitude and compared to test data obtained from the actuators. The total force approximation of the pressure cells was performed by assuming a linear downward pressure distribution, extrapolating to the mid height of the soil, multiplying each cell by its tributary width and soil depth of 3 ft (0.91 m), and summing the forces together. As shown in Figure 38, the pressure cells appear to have been relatively accurate at the beginning and final test movements; however, the cells overestimated the measured actuator pressure for displacements from 0.5 to 3.0 inches by a factor as large as 1.6. Although these cells seem to have over-registered the pressure magnitudes, the pressure distributions and movements can still be analyzed to examine the general soil pressure behavior.

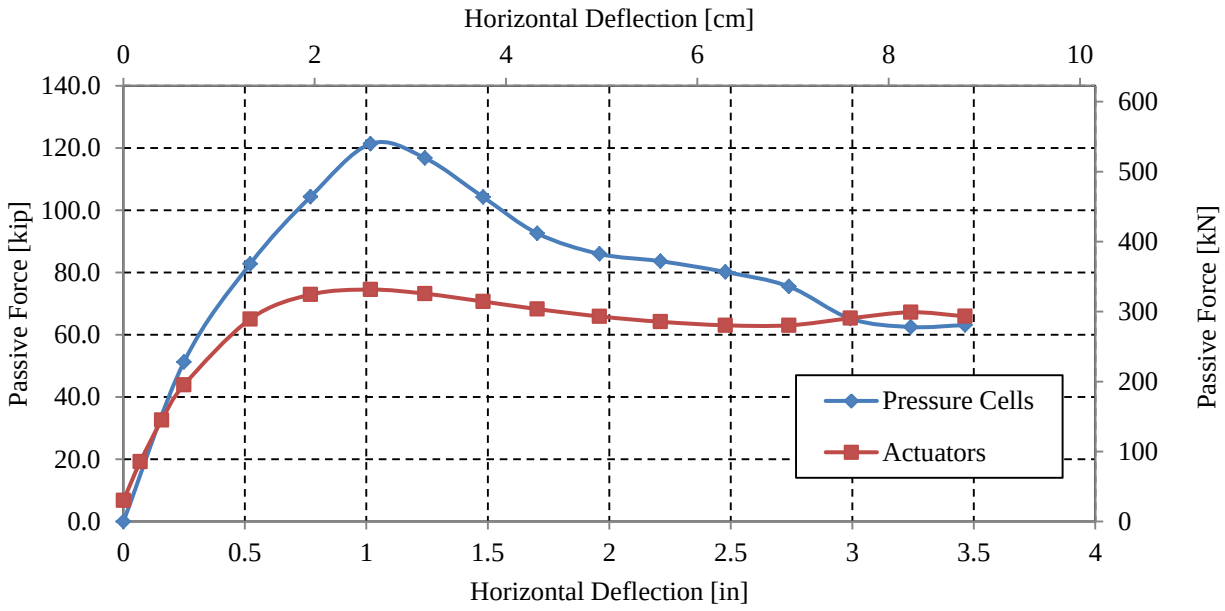

Figure 38. Passive force vs. deflection curve as estimated by the pressure cells and recorded by the actuators for the 30° skew test.

Applied Shear Force vs. Transverse Displacement

The relationship between the applied shear force (P_T) and transverse displacement is plotted in Figure 39. The applied shear force was computed using Equation (3) and displacement values were based on shape array measurements taken during testing. The shape arrays measured positive-east and negative-west. The acute side of the skew was on the west.

Although the results for the 15° and 30° skews appear to be reasonable, the 45° skew test looks highly irregular. In this test, problems in controlling the actuators led to initial movement towards the east, toward the obtuse angle of the skew. This is opposite to the results of nearly all of the other skew tests performed at this site. Though it was previously mentioned that the 45° skew shape array test did not have reliable shape array calibration, the deflections are likely within 10%. It is assumed that the unusual easterly movement occurred because this test was the first of these tests performed with backfill in almost a year. Some type of catch under the cap, a kink in the shape array, or simply finding equilibrium with the

actuators during the performance of the test could have caused the 0.07 inch displacement to the east until the passive force peak was reached. After the peak, the cap began moving to the west, as was seen in other tests.

Despite the irregularity in the displacement pattern, the shear force values themselves follow the same pattern for the 45° skew test as for both the 15° and 30° skew tests, with an initial peak which drops before again increasing in shear with transverse displacement. The final slopes of all three tests are similar. As the skew angle increased, the peak shear force also increased from 15° to 30° to 45° (see Figure 39 [A] despite the fact that the longitudinal force was progressively decreasing as the skew angle increased. The higher shear forces also resulted in greater transverse movements toward the acute side of the pile cap as the skew angle increased for the 15 and 30° skew tests. In Figure 39 [B] the shear force for each cap has been normalized by the maximum shear force. The curves for the 15° and 30° skew tests are very similar and the maximum shear force developed with a transverse displacement of a couple hundredth of an inch. The maximum shear force occurred at the maximum longitudinal force. Once this resistance was reached, transverse movement occurred more freely, resulting in the flatter portions of the curves as seen in Figure 39 [A] and [B] below.

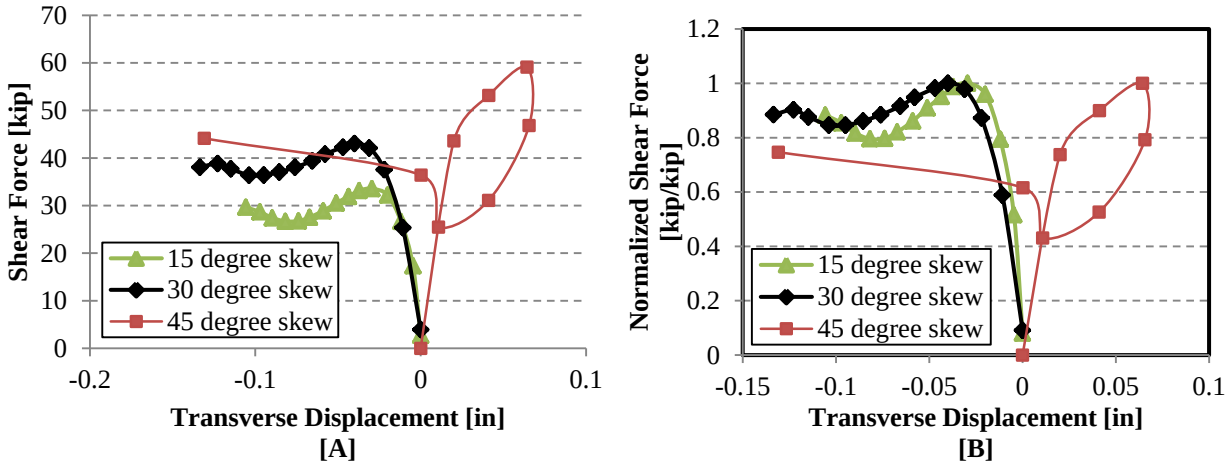

Figure 39. [A] Applied shear force versus transverse displacement; [B] Normalized applied shear force versus transverse displacement

According to Duncan and Mokwa (2001), the amount of movement required to mobilize skin friction on an interface is typically between 0.10 and 0.25 inch. Therefore, the applied shear force could be less than the shear resistance (P_R) provided by the abutment wall. In a subsequent report the shear resistance will be calculated once the interface friction angle and cohesion on the pile cap have been more accurately assessed.

Shear Plane Geometry

The location of failure planes in the backfill for the tests on the 0°, 15°, 30°, and 45° skews are provided in Figures 37, 38, 39 and 40, respectively. The failure plane locations were obtained by observing the offset in the red sand columns positioned throughout the backfill. The measured heave of the backfill is also shown on each figure.

The 0°, 15°, and 30° tests all showed a top surface plane which extended from the top of the face of the pile cap down to meet with the failure plane coming from the bottom of the pile cap. The lower failure planes on all four tests extended out nearly horizontally from the wall, with the 30° test extending down a small amount, then angling up to break the surface roughly 10 ft from the pile cap.

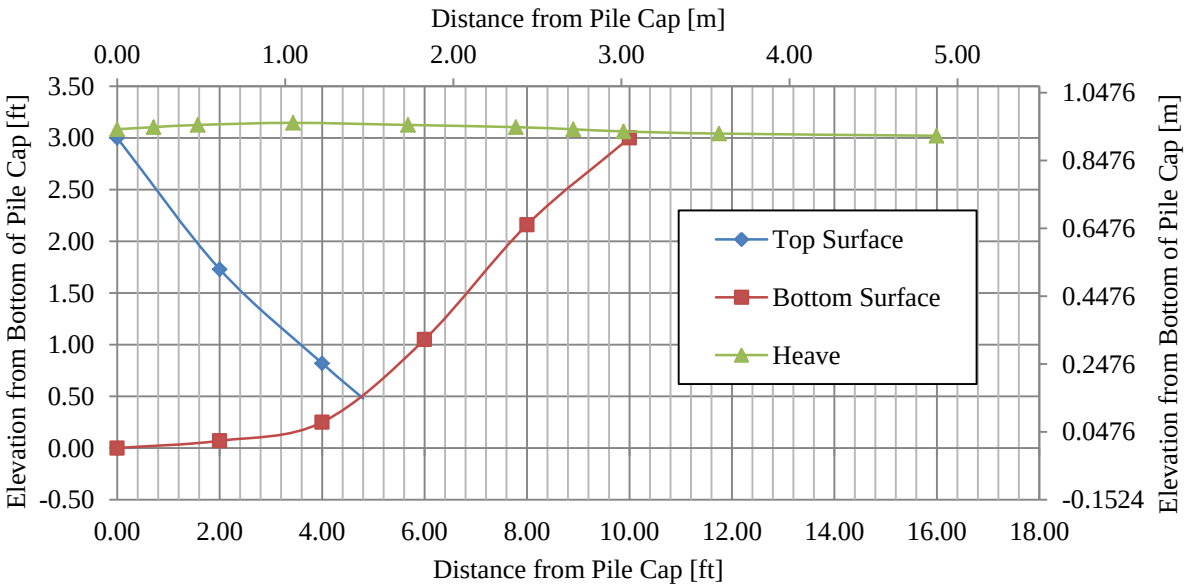

Figure 40. Shear plane geometry and Ground surface heave for 0° skew test.

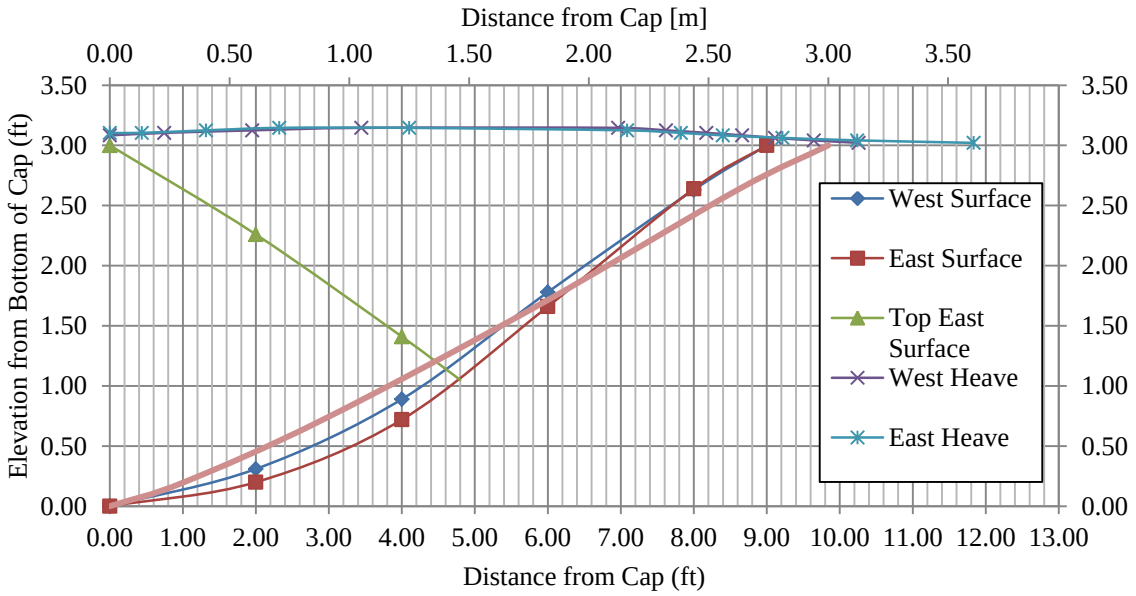

Figure 41. Shear plane geometry and Ground surface heave for 15° skew test.

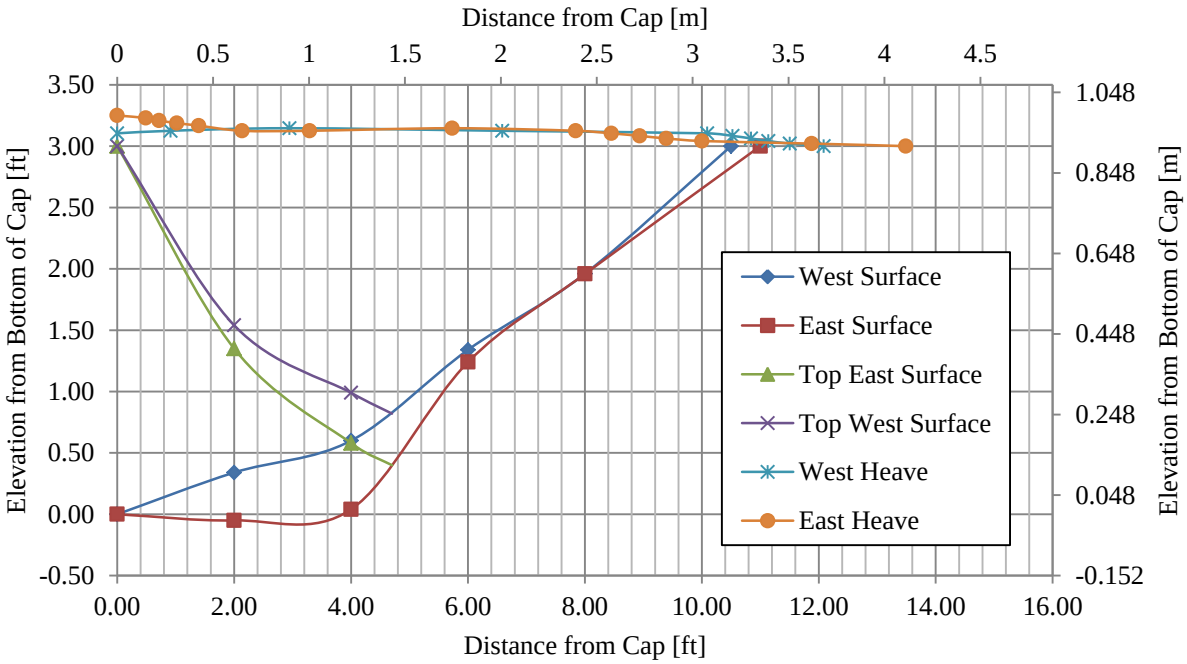

Figure 42. Shear plane geometry and Ground surface heave for 30° skew test

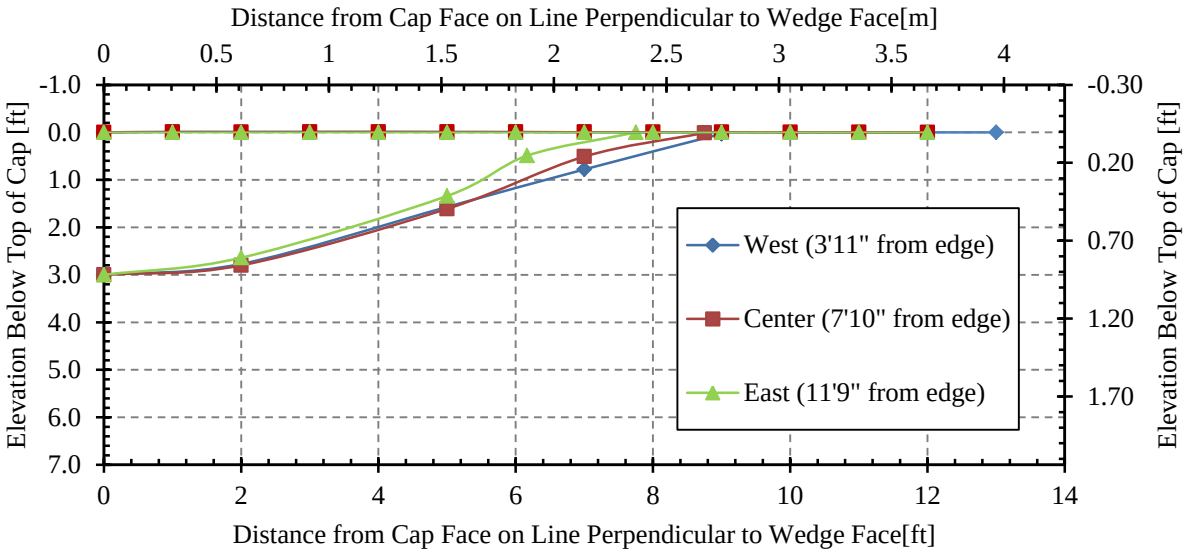

Figure 43. Shear plane geometry 45° 3 foot skew test

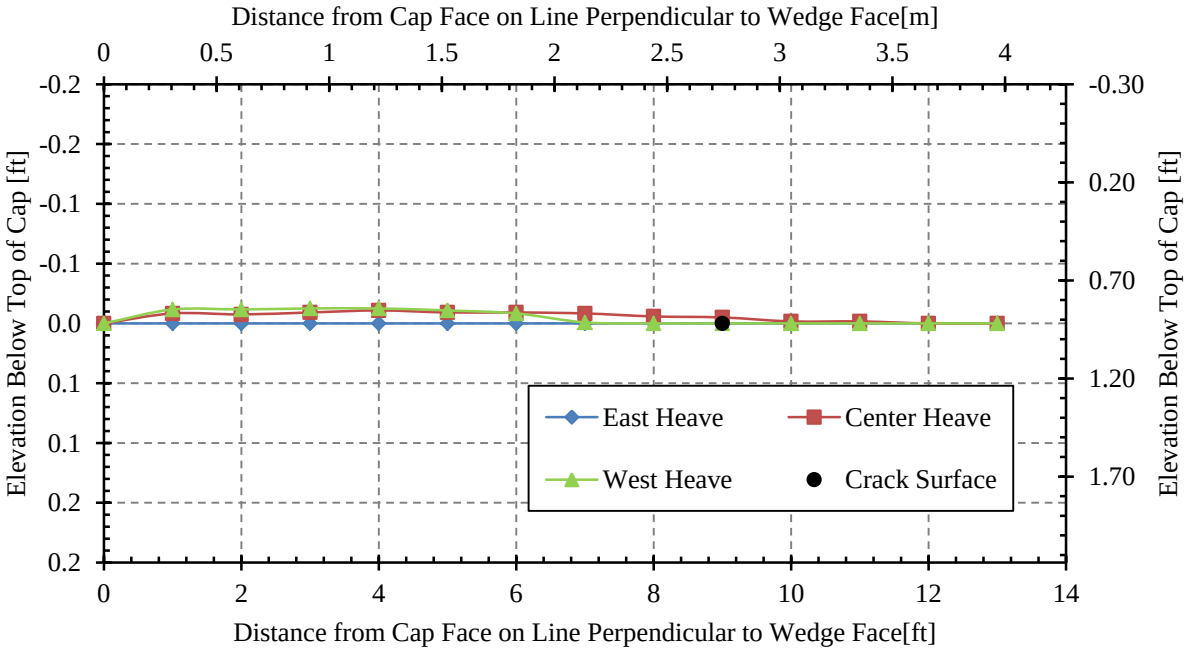

Figure 44. Ground surface heave for 45° 3 foot skew test

For the 45° skew test ground surface heave was plotted along three lines perpendicular to the face of the abutment back. Figure 41 provides a more detailed view of the heave on each of these lines.

Heave was lowest on the eastern cross-section and higher for the center and west cross-sections. The maximum heave occurred between 2 and 4 feet back from the wall face and decreased to zero where the failure surface daylighted and for points on the backfill surface beyond this boundary.

The drained friction angle, ϕ', for each test was derived based on equation (8) where the angle α represents the angle of the linear portion of the failure surface relative to the horizontal.

$$\alpha = 45 - \phi'/2 \tag{8}$$

Backfill from all three skewed tests had very similar friction angles with the 15°, 30°, and 45° skews having friction angles of 46°, 44°, and 44° respectively.

CONCLUSIONS

1. 1. Results of this large-scale field study confirm that passive force decreases significantly as the abutment skew angle increases from 15° to 30° and then 45° relative to non-skewed walls as observed in small-scale lab test results (Rollins and Jessee, 2013) and numerical models (Shamsabadi et al, 2006) for densely compacted granular backfill.
2. The passive-force reduction curve proposed by Rollins and Jessee (2013) appears to provide a reasonable estimate of the measured passive force reduction in densely compacted granular material despite the larger backwall width to height ratio (3.7) in these tests relative to the ratio of 2.0 used in previous testing. These results suggest that W/H ratios do not strongly influence the reduction in passive force.
3. Despite the reduction in passive force attributable to the increase in skew angle, the initial stiffness of the passive force-deflection curves was relatively unaffected by skew angle. In addition, the displacement required to develop the peak passive force was about 3% of the wall height for the 0°, 15°, 30° and 45° degree skew tests.
4. Backwall pressure distribution is nonlinear. The largest pressures were located near the edges and lowest pressures were located near the center of the backwall face; however, the largest pressures developed on the obtuse side of the backwall due to counter-clockwise rotation of the cap.

ACKNOWLEDGMENTS

Funding for this study was provided by an FHWA pooled fund study supported by Departments of Transportation from the states of California, Minnesota, Montana, New York, Oregon, and Utah. Utah served as the lead agency with David Stevens as the project manager. This support is gratefully acknowledged; however, the opinions, conclusions and recommendations in this paper do not necessarily represent those of the sponsoring organizations. We also express appreciation to the Salt Lake City Airport Department for providing access to the test site used in this study.

REFERENCES

AASHTO (2011). "Guide Specifications for LRFD Seismic Bridge Design." 5th Edition, 3-106.

Apirakyorapinit, P., Mohammadi, J., and Shen, J. (2012). "Analytical Investigation of Potential Seismic Damage to a Skewed Bridge." *Practice Periodical on Structural Design and Construction*, 16(1), 5-12.

Burke Jr., M. P. (1994). "Semi-Integral Bridges: Movements and Forces." 1-7.

Caltrans (2001). "Seismic Design Criteria Version 1.2." California Department of Transportation, Sacramento, California.

Duncan, J. M., and Mokwa, R. L. (2001). "Passive Earth Pressures: Theories and Tests." *Journal of Geotechnical and Geoenvironmental Engineering, ASCE*, 127(3), 248-257.

Elnashai, A. S., Gencturk, B., Kwon, O., Al-Qadi, I. L., Hashash, Y., Roesler, J. R., Kim, S. J., Jeong, S., Dukes, J., and Valdivia, A. (2010). "The Maule (Chile) Earthquake of February 27, 2010: Consequence Assessment and Case Studies." Department of Civil and Environmental Engineering, University of Illinois at Urbana-Champaign, 190.

Lee, K. L., and Singh, A. (1971). "Relative Density and Relative Compaction." *Journal of Soil Mechanics and Foundations Design*, 97(7), 1049-1052.

Mokwa, R. L., and Duncan, J. M. (2001). "Experimental Evaluation of Lateral-Load Resistance of Pile Caps." *Journal of Geotechnical and Geoenvironmental Engineering, ASCE*, 127(2), 185-192.

Rollins, K. M., and Cole, R. T. (2006). "Cyclic Lateral Load Behavior of a Pile Cap and Backfill." *Journal of Geotechnical and Geoenvironmental Engineering, ASCE*, 132(9), 1143-1153.

Rollins, K. M., Gerber, T., Cummins, C., and Herbst, M. (2009). "Monitoring Displacement vs. Depth in Lateral Pile Load Tests with Shape Accelerometer Arrays." *Proceedings of 17th International on Soil Mechanics & Geotechnical Engineering*, 3, 2016-2019.

Rollins, K. M., Gerber, T. M., Cummins, C. R., and Pruett, J. M. (2010). "Dynamic Pressure on Abutments and Pile Caps." *Report No. UT-10.18*, B. Y. University, U. D. o. Transportation, and F. H. Administration, eds., Utah Department of Transportation, 255.

Rollins, K. M., Gerber, T. M., and Heiner, L. (2010). "Passive Force-Deflection Behavior for Abutments with MSE Confined Approach Fills." *Report No. UT-10.15*, Utah Department of Transportation.

Rollins, K. M., and Jessee, S. (2012). "Passive Force-Deflection Curves for Skewed Abutments." *Journal of Bridge Engineering*, ASCE, 17(5).

Rollins, K. M., and Sparks, A. E. (2002). "Lateral Load Capacity of a Full-Scale Fixed-Head Pile Group." *Journal of Geotechnical and Geoenvironmental Engineering, ASCE*, 128(9), 711-723.

Sandford, T. C., and Elgaaly, M. (1993). "Skew Effects on Backfill Pressures at Frame Bridge Abutments." *Transportation Research Record: Journal of the Transportation Research Board*, 1-11.

Shamsabadi, A., Kapuskar, M., and Zand, A. (2006 Published). "Three-Dimensional Nonlinear Finite-Element Soil-Abutment Structure Interaction Model for Skewed Bridges." *Paper presented at 5th National Seismic Conference On Bridges and Highways*, 1-10.

Shamsabadi, A., Rollins, K. M., and Kapaskur, M. (2007). "Nonlinear Soil-Abutment-Bridge Structure Interaction for Seismic Performance-Based Design." *Journal of Geotechnical and Geoenvironmental Engineering, ASCE*, 133(6), 707-720.

Steinberg, E., and Sargand, S. (2010). "Forces in Wingwalls from Thermal Expansion of Skewed Semi-Integral Bridges." *Report No. FHWA/OH-2010/16*, Prepared by Ohio University for Ohio Department of Transportation, Athens, OH, 87.

Strassburg, A. N. (2010). "Influence of Relative Compaction on Passive Resistance of Abutments with Mechanical Stabilized Earth (MSE) Wingwalls." M.S. Thesis, Brigham Young University, Provo, UT.

Unjohn, S. "Repair and Retrofit of Bridges Damaged by the 2010 Chile, Maule Earthquake." *Proc., International Symposium on Engineering Lessons Learned from the 2011 Great East Japan Earthquake*, Tokyo, Japan.